Pathological angiogenesis requires Syndecan-4 for efficient VEGFA-induced VE-Cadherin internalization

Giulia De Rossi[1,5] *, Maria Vähätupa[2], Enrico Cristante[3], Samantha Arokiasamy[1], Sidath E. Liyanage[3], Ulrike May[2], Laura Pellinen[2], Hannele Uusitalo-Järvinen[2], James W. Bainbridge[3,4], Tero A.H. Järvinen[2] and James R. Whiteford[1] *.

Affiliations: [1]William Harvey Research Institute, Barts and The London School of Medicine and Dentistry, Queen Mary University of London, Charterhouse Square, London EC1M 6BQ, United Kingdom.

[2]Faculty of Medicine & Health Technology, Tampere University, 33014 Tampere, Finland & Departments of Orthopedics & Traumatology and Tampere Eye Centre, Tampere University Hospital, 33521 Tampere, Finland.

[3]UCL Institute of Ophthalmology, Genetics department, 11-43 Bath Street, London EC1V 9EL, UK.

[4]NIHR Biomedical Research Centre at Moorfields Eye Hospital NHS Foundation Trust, City Road, London EC1V 2PD, UK.

[5]UCL Institute of Ophthalmology, Department of Cell Biology, 11-43 Bath Street, London EC1V 9EL, UK.

Running title: VE-Cadherin and Syndecan-4 in Angiogenesis

Corresponding authors:

JRW, j.whiteford@qmul.ac.uk , William Harvey Research Institute, Queen Mary University of London, Charterhouse Square, London EC1M 6BQ, UK. Tel: +44(0)2078823909;

GDR, giulia.derossi@ucl.ac.uk , UCL Institute of Ophthalmology, Department of Cell Biology, 11-43 Bath Street, London EC1V 9EL, UK. Tel: +44(0)2076084016

Key words: Angiogenesis, Cadherin, Vascular Endothelial growth factor, Syndecan, vascular permeability.

Subject terms: Angiogenesis, Animal Models of Human Disease, translational studies, cell biology/structural biology, vascular disease.

Word count: 6,736

Total number of figures and tables: 7

TOC category: Translational

TOC subcategory: Vascular biology

ABSTRACT

Objective: Vascular endothelial growth factor (VEGFA) and its receptor VEGFR2 drive angiogenesis in a number of pathologies, including diabetic retinopathy, wet age-related macular degeneration and cancer. Studies suggest roles for heparan sulfate proteoglycans (HSPG) in this process although the nature of this involvement remains elusive. Here, we set to establish the role of the HSPG Syndecan-4 (SDC4) in pathological angiogenesis.

Approach and Results: We report that angiogenesis is impaired in mice null for SDC4 in models of neovascular eye disease and tumor development. Our work demonstrates that SDC4 is the only syndecan whose gene expression is upregulated during pathological angiogenesis and is selectively enriched on immature vessels in retinas from diabetic retinopathy patients. Combining *in vivo* and tissue culture models, we identified SDC4 as a downstream mediator of functional angiogenic responses to VEGFA. We found that SDC4 resides at endothelial cell (EC) junctions, interacts with VE-Cadherin and is required for its internalization in response to VEGFA. Finally, we show that pathological angiogenic responses are inhibited in a model of wet age-related macular degeneration by targeting SDC4.

Conclusions: We show that SDC4 is a downstream mediator of VEGFA-induced VE-Cadherin internalization during pathological angiogenesis and a potential target for anti-angiogenic therapies.

GRAPHIC ABSTRACT:

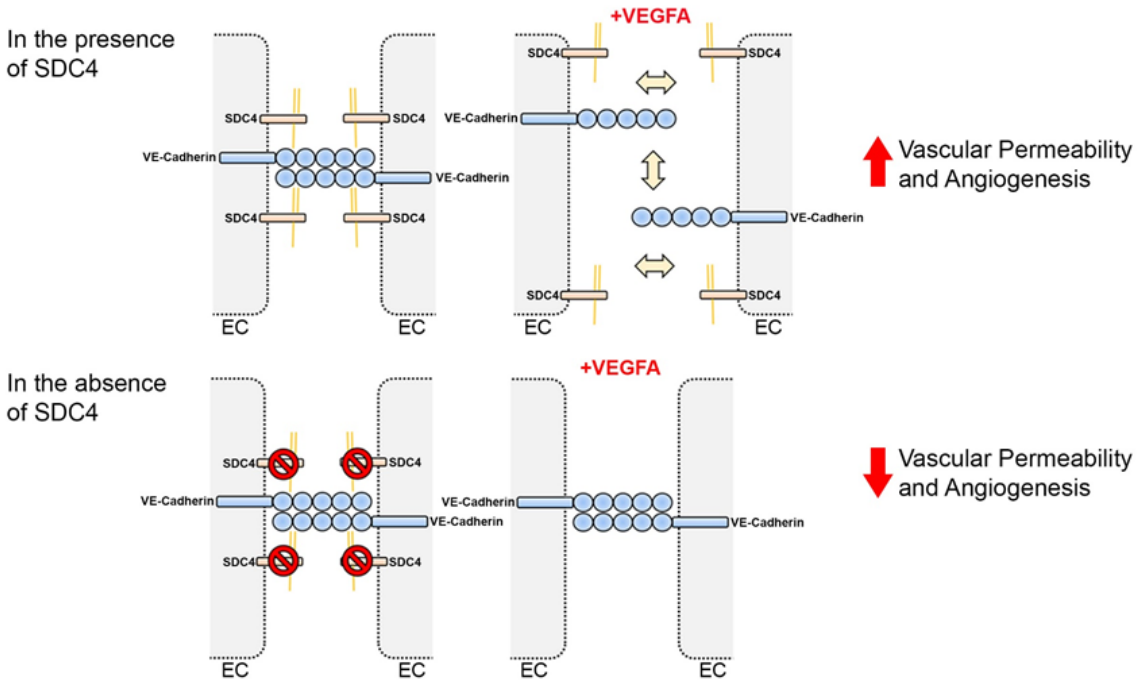

ABBREVIATIONS

CNV	Choroidal neovascularization
DMBA	7,12-Dimethylbenz(a)anthracene
EC	Endothelial Cell
eGFP	Enhanced Green Fluorescent Protein
Erk	Mitogen-activated Protein Kinase
FBS	Fetal Bovine Serum
HS	Heparan Sulfate
HSPG	Heparan Sulfate Proteogylcan
HUVECs	Human Umbilical Vein Endothelial Cells
Lectin GS-II	Lectin GS-II from *Griffonia simplicifolia*
NF-κB	Nuclear Factor Kappa-light-chain-enhancer of activated B cells
OIR	Oxygen Induced Retinopathy
rtPCR	Reverse Transcriptase Polymerase Chain Reaction
SDC	Syndecan
TPA	Phorbol Ester
VE-Cadherin	Vascular Endothelial Cadherin
VEGFA	Vascular Endothelial Growth Factor A
VEGFR2	Vascular Endothelial Growth Factor Receptor 2
WT	Wild-Type

INTRODUCTION

Angiogenesis is a critical developmental process and an essential component of physiological tissue regeneration [1]. In the pathogenesis of neovascular eye diseases, cancer and inflammatory disorders, new blood vessel formation is a key feature and significant efforts have been made to control this process for therapeutic benefit [2-6]. The pro-angiogenic cytokine vascular endothelial growth factor A (VEGFA) and its receptor VEGFR2 regulate angiogenesis in these pathologies; promoting endothelial cell (EC) survival, proliferation and migration [7]. The movement of ECs during new vessel growth depends on the remodeling of EC junctions and VEGFA has a crucial role in regulating the junctional concentration of vascular endothelial cadherin (VE-Cadherin) [8-12]. The presence of a heparin binding domain on the most biologically active isoform of VEGFA, $VEGFA^{164/165}$, is suggestive of a role for heparan sulfate proteoglycans (HSPGs) in angiogenesis, particularly in facilitating the engagement of ligand with receptor [13, 14]. For this reason the four-member syndecan family of HSPGs have been proposed to have roles in this process [15]. Syndecans consist of a short cytoplasmic domain, a single-pass transmembrane domain and a larger extracellular core protein which is substituted with predominantly HS chains. Numerous interactions with these sugars and bioactive molecules such as growth factors and extracellular matrix molecules have been reported [16-19]. Recent studies have shown syndecan-2 (SDC2) forms a tri-molecular complex with $VEGFA^{165}$ and VEGFR2 leading to enhanced signaling. In contrast, syndecan-4 (SDC4), the family member most closely related to SDC2, has no impact on VEGFA signaling. This difference was linked to enhanced 6-O-sulfation on SDC2 HS chains which is determined by unique sequence motifs contained in the extracellular core protein of SDC2 [20]. Several studies have identified a pro-angiogenic role for SDC4 in response to stimuli such as FGF2 and Prostaglandin E_2 and adult *Sdc4-/-* mice exhibit defects in the development of fetal vessels in the placental labyrinth and in angiogenesis during granulation tissue formation after wounding [21-25]. All of which, is suggestive of a functional requirement for SDC4 in new blood vessel formation.

Here, we set out to elucidate the function of SDC4 in VEGFA-driven pathological angiogenesis using a variety of disease models. We found that *Sdc4-/-* animals are protected in both murine models of neovascular eye disease and skin tumor models. SDC4 gene expression, unlike that of other family members, increases during pathological angiogenesis but not during developmental angiogenesis in mice, and is selectively expressed on immature blood vessels in retinas of diabetic retinopathy patients. Functional assays, such as VEGFA-induced *ex vivo* sprouting and cell migration demonstrate a strong requirement for SDC4, although VEGFR2 signaling in response to VEGFA is normal in *Sdc4-/-* null ECs. We show that SDC4 acts downstream of VEGFA/VEGFR2, and is required for efficient VE-Cadherin trafficking away from EC junctions in response to VEGFA. Finally, we demonstrate that targeting SDC4/VE Cadherin interaction in a pre-clinical model of Wet Age-Related Macular Degeneration leads to inhibition of pathological angiogenesis. These findings identify SDC4 as an important regulator of VE-Cadherin trafficking in VEGFA-driven junctional reorganization, an essential component of pathological angiogenesis, and as such has the potential to be targeted for therapeutic benefit.

MATERIALS AND METHODS

Please see the Major Resources Table and additional Materials and Methods in the Supplemental Material.

Experimental animals: *Sdc4-/-* mice (on a C57BL/6J background)[22] were obtained from the Centre for Animal Resources and Development (CARD, Kunamoto University, Japan) with the kind permission of Professor Tetsuhito Kojima (Nagoya University, Japan). All adult mice were used at an age between 5-8 weeks at an average weight of 25 g. As appropriate, age-matched control mice were littermates or C57BL/6J wild-type mice purchased from Charles River. Unless stated male animals were used in these studies, since the differences between males and females in the models used is negligible. Animals were housed and treated in Accordance with UK Home Office Regulations and all experiments were approved by the UK Home Office according to the Animals Scientific Procedures Act 1986 (ASPA) and by the National Animal Ethics Committee of Finland.

Developmental angiogenesis mouse model: Neonatal WT, *Sdc4+/-* and *Sdc4-/-* littermates (both male and female) were euthanized at P6 and retinal flat mounts were prepared for lectin GS-II staining. Briefly, retinas were washed extensively in PBS, blocked in 3% BSA followed by overnight staining with lectin GS-II-Alexa594 and an anti-αSMA-alexa488 antibody (1:150, Sigma, in-house conjugated) in 0.5% triton in PBS. Retinas were imaged using confocal microscopy (Carl Zeiss LSM 700) with 10× objective. The rate of developmental angiogenesis at P6 was determined by measuring the diameter of vasculature via the optic nerve to the tips of the blood vessels. Two measurements per retina were taken and an average was calculated.

Oxygen-induced retinopathy (OIR) mouse model: Neonatal mice (both male and female) at P7 were exposed to 75% oxygen for 5 days with their nursing mothers. At P12, they were returned to normoxia. Animals were euthanized at P12 to determine the area of vaso-obliteration or at P17 to determine the rate of retinal revascularization and pre-retinal neovascularization [26, 27]. As postnatal weight gain has been shown to affect outcome in the OIR model [28], only weight matched (±1 g) pups were used in each experiment. Analysis of retinal vasculature was done as previously described [29]. Briefly, eyes were enucleated, fixed with 4% PFA for one hour and retinas dissected. Flat mount retinas were blocked in 10% normal goat serum and 10% fetal bovine serum for 2 hours, incubated overnight with isolectin GS-IB_4 (1:100). Briefly, retinas were imaged using confocal microscopy (Carl Zeiss LSM 700) with 10× objective. Pre-retinal neovascular tufts were readily distinguished from the superficial vascular plexus by focusing just above the inner limiting membrane. Areas of vascular obliteration and pathological neovascularization (neovascular tufts) were quantified using Adobe Photoshop CS3.

Laser-induced choroidal neovascularization (CNV) mouse model: WT and *Sdc4-/-* 6 week old male mice were anesthetized by intraperitoneal injection of 0.15 ml of a mix of Domitor and Ketamine and pupils dilated with topical administration of 1 % Tropicamide and 2.5 % Phenylephrine. Three burns per eye were be made by laser photocoagulation (680 nm; 100 µm spot diameter; 100 ms duration; 210 mW). Only burns that produced a bubble, indicating the rupture of the Bruch's membrane, were counted in the study. At day 7 after the laser injury, fundus fluorescein

angiography (FFA) was performed to measure the area of CNV lesion. The area of lesion was then quantified using Imaris Software (Bitplane) and expressed as number of pixels. Additionally, at the end of the experiment (day 7) mice were culled, choroid-RPE tissue dissected, flat-mounted and stained with lectin GS-II. Confocal images were then acquired using a PASCAL laser-scanning confocal microscope (Carl Zeiss) followed by volumetric analysis with Imaris software (Bitplane).

B16F1 melanoma tumor model: B16F1 mouse melanoma cells were obtained from HPA Laboratories (UK) and $5x10^7$ cells/ml in 100 µl of PBS were injected sub-cutaneously into the left flank of 6 week old male WT and *Sdc4-/-* mice (n=12 per group). Mice were left for 7 or 14 days prior to sacrifice by cervical dislocation. A longitudinal incision was made from the chest to the genital area, skin was peeled and pinned down and tumors were revealed. Photographs were taken with a digital camera and tumors excised using scalpel and tweezers. Samples were then weighed on a precision balance and diameter measured using a ruler. Samples were then snap frozen in liquid nitrogen and stored at -80 °C.

Skin tumor induction: *Sdc4-/-* and C57BL/6 WT male mice were treated with DMBA and TPA to induce skin tumors according to the established protocol[30-32]. In brief, the backs of 8 week old mice were shaved and 24 h later 50 µg DMBA (7,12-Dimethylbenz[a]anthracene) (Sigma, Dorset, UK) in 200 µl acetone was applied topically on the shaved area of the dorsal skin. After a week, the back skin of the mice was treated twice a week with 5 µg TPA (12-O-tetradecanoylphorbol-13-acetate) (Sigma) in 200 µl acetone for 21 weeks. Tumors (1 mm in diameter or larger) were counted twice a week. The fur excluding tumors was carefully shaved every two weeks.

VE-Cadherin internalization assay: Cells were serum starved for 3 hours prior to incubation for 1 hour at 4 °C in the presence of an anti-VE-Cadherin antibody (clone BV13, eBioscience) conjugated in-house to Alexa555. Unbound antibody was washed away using serum free medium. 30 ng/ml of VEGFA was added to cells for 5 min at 37 °C to allow internalization of VE-Cadherin and bound antibody. For analysis of internalized VE-Cadherin, cell surface bound antibody was removed using an acid wash (glycine 25 mM, 3% BSA in PBS, pH 2.7). Cells were washed 3X with ice cold PBS and fixed with 4 % PFA, 0.25 % glutaraldehyde prior to analysis by confocal microscopy.

Proximity ligation assay: Proximity ligation assay or PLA is a technique that allows the identification *in situ* of spots in which 2 proteins are in close proximity (less than 40 µm). The PLA experiments were performed as per manufacturer's instructions (Duolink, Sigma Aldrich). Cells were treated as indicated in the results section. Following treatments, medium was taken off, cells were washed in PBS at RT, fixed in 4 % PFA for 15 min at RT. After a 5 min wash in PBS, PFA was quenched by incubating cells with 0.1 M NH4CL for 10 min at RT.

Evans blue permeability assay: 6-8 week old male mice were anesthetized by i.m. injection of 1 ml/kg ketamine (40 mg) and xylazine (2 mg) in saline solution. The back skin was shaved using an electric razor. Mice then received Evans Blue dye (0.5 % in PBS, 5 µl per g bodyweight) i.v. through the tail vein. Afterwards, 50 µl of PBS containing either 100 ng of VEGFA or 100 µg of Bradykinin or PBS alone were

injected s.c. in the mouse dorsal skin. After 90 min animals were sacrificed by cervical dislocation. Dorsal skin was removed and injected sites were cut out as circular patches using a metal puncher (~8 mm in diameter). Samples were then incubated in 250µl of formamide at 56 °C for 24 h to extract Evans Blue dye from the tissues. The amount of accumulated Evans Blue dye was quantified by spectroscopy at 620 nm using a Spectra MR spectrometer (Dynex technologies Ltd., West Sussex, UK). Results are presented as the optical density at 620 nm (OD620) per mg tissue and per mouse.

Statistical analysis: Data are presented as mean ± s.e.m. and sample sizes are reported in each figure legend. Each experiment on animals was performed on at least two independent litters of a given genotype. Data were plotted and analyzed for statistical significance using Prism 6 (Graphpad software Inc.). Welch's t-test was used when two independent groups were compared. Parametric statistical tests (two-tailed t-test and one- or two-way ANOVA) were used to compare the averages of two or more groups. Normality and variance were not tested to determine whether the applied parametric tests were appropriate. Bonferroni post-hoc test was used when we were interested in a set number of planned comparisons (i.e. Control vs Mutant(s)). Tukey post-hoc test was used when wanting to make unplanned pairwise comparisons (i.e. time-points). Spearman's rank correlation test was conducted to test correlation between multiple variables. P-values less than 0.05 were considered statistically significant.

RESULTS

SDC4 is dispensable for vascular development but essential for pathological angiogenesis

As with other syndecan family members, adult *Sdc4-/-* animals show no abnormalities and are phenotypically comparable to wild-type (WT) littermates which is suggestive of normal development. In accordance with this hypothesis and in keeping with a recent study [20], we observed no major differences in postnatal retinal vascular development between WT, *Sdc4+/-* and *Sdc4-/-* P6 neonates (Figure 1A and B). This was also reflected by the absence of any differences in the number of arteries and veins between the genotypes (Figure IA in Data Supplement). Analysis of parameters such as vessel size (Figure IB and IC in Data Supplement), density (Figure ID in Data Supplement), and pericyte coverage (Figure IE in Data Supplement) in additional adult vascular beds (skin, muscle and connective tissue, Figure IF in Data Supplement) confirmed that *Sdc4-/-* animals developed a normal vascular network indicating that angiogenesis during development was not affected in *Sdc4-/-* mice.

We next examined whether angiogenic responses in disease models were affected by genetic deletion of SDC4. Oxygen-induced retinopathy (OIR) is a hypoxia-driven angiogenesis model that recapitulates features of diabetic retinopathy and retinopathy of prematurity[33]. OIR was performed on 7-day old WT and *Sdc4*-/- pups by exposing them to hyperoxia (75 % O_2 for 5 days) leading to the abolition of the retinal vasculature, before being returned to normoxia which stimulates a neovascular response. Exposure to oxygen led to a comparable loss in retinal vasculature in both *Sdc4-/-* and WT control littermates (Figure IIA and B in Data Supplement); however, upon return to normoxic conditions it was evident that the formation of neovascular tufts (a hallmark of pathological angiogenesis) was significantly reduced (~ 40% decrease) in the retinas of *Sdc4-/-* mice compared to WT mice (Figure 1C and D). In contrast, the physiological neovascular response associated with hypoxia in *Sdc4-/-* animals was only slightly increased as determined by smaller avascular areas in these animals 5 days post-hyperoxia compared to WT littermates (Figure IIC and D in Data Supplement). We next investigated whether neovascularization was also attenuated in *Sdc4-/-* mice in the laser-induced choroidal neovascularization (CNV) model which mimics neovascular ('wet') age-related macular degeneration [34]. Laser photocoagulation was performed on the eyes of 6-week old WT and *Sdc4-/-* littermates to stimulate a neovascular response in the choroid. Areas of CNV measured 7 days after injury by fluorescein angiography were found to be significantly smaller in the eyes of *Sdc4-/-* mice compared to WT mice (Figure 1E and F). CNV lesions were predominantly composed of ECs on the basis of lectin GS-II staining and we confirmed the reduction in lesion volume (~80% decrease) in *Sdc4-/-* mice using 3D confocal reconstruction (Figure 1G and H). Together, this data highlights the requirement for SDC4 in promoting vessel growth in two models of neovascular eye disease.

Angiogenic defects are not restricted to ocular disease models in *Sdc4-/-* mice

We next set out to establish whether the angiogenic defects observed in *Sdc4-/-* mice were restricted to ocular neovascularization or would extend to angiogenic-

driven tumor development models. In the first instance, we injected B16F1 melanoma cells (which express SDC4, Figure IIIA in Data Supplement) into the flank of WT and *Sdc4-/-* mice. Animals were sacrificed after 2 weeks and both tumor volume and tumor weight were significantly reduced in the *Sdc4-/-* mice compared to WT controls (Figure 2A and B; Figure IIIB in Data Supplement). Critically, immunofluorescence staining of tumor sections for EC specific markers CD31 and Podycalyxin revealed vascular structures, with in many cases, a well-defined lumen (white arrows in Figure 2C and D; Figure IIIC and D in Data Supplement), whereas in tumors from *Sdc4-/-* mice, ECs failed to organize into tubules and were more sparsely distributed (Figure 2C and D; Figure IIIC and D in Data Supplement). We next tested whether this was also the case in a model of epidermal papilloma formation induced by two stage treatment with DMBA and TPA, the progression of which, is angiogenesis-dependent [30, 35]. At the end point of 19-weeks, WT animals had on average 2.4 times more tumors than *Sdc4-/-* mice and the incidence of large tumors was 6-fold higher (Figure 2E and F). In the DMBA/TPA model, tumor angiogenesis takes place first by increased blood vessel density and later, during papilloma formation, by increased blood vessel diameter. Histochemical staining for the EC marker CD31 revealed smaller blood vessel lumens in tumors formed in *Sdc4-/-* mice compared to WT (Figure 2G; Figure IIIE in Data Supplement). Together this data provides compelling evidence that the role of SDC4 in pathological angiogenesis is not restricted to neovascular eye disease, but also extends to tumor development.

SDC4 is upregulated during pathological angiogenesis

To understand further the role of SDC4 in pathological angiogenesis, we next compared syndecan gene expression in both the context of developmental and pathological angiogenesis in the murine retina. During the early stages of murine postnatal development, angiogenesis occurs in the eye leading to the formation of a superficial retinal vascular plexus and in C57BL/6 mice this occurs during the first 8 days after birth. Quantitative rtPCR was performed on retinal mRNA from day P0, 4, and 7 neonates to measure the expression of SDC1, -2, -3 and -4 during development. SDC1 and -3 showed downregulated expression over time, whereas SDC2 and -4 remained unchanged (Figure 3A). Next, we examined the transcript profile of syndecans in a murine model of retinal pathological neovascularization. When pups were subjected to OIR, we detected a marked increase in SDC4 gene expression in retinas at P17, the time point at which neovascularization peaks, whereas the expression of the other 3 syndecans remained stable (Figure 3B). Interestingly, this was also the case in both the laser CNV model and in B16F1 melanomas. SDC4 gene expression was upregulated in retinas 7 days post laser injury as compared to control retinas (Figure IVA in Data Supplement). This was also the case when SDC4 gene expression was analyzed in B16F1 melanomas (7 days post injection), when compared to B16F1 cells in culture (Figure IVB in Data Supplement). These increases in gene expression were not a characteristic of the other SDC family members, the exception being SDC3 in the B16F1 melanoma model, which according to previous studies, could be immune cell derived[36].

To investigate whether SDC4 was upregulated in a human disease setting, we analyzed its expression in the retinal neovascular membranes that develop in human diabetic retinopathy patients. Neovascular membranes were collected from type I

diabetes patients suffering from retinopathy, who had either already developed or had threatening tractional retinal detachment due to fibro-vascular proliferation. These tissue samples represented the end stage of the disease, but still contained regions with active pathological angiogenesis. Histological analysis of adjacent tissue sections revealed SDC4 expression predominantly associated with blood vessels ($CD31^+$ areas). Moreover, immunostaining for VEGFR2 (a marker of pathological immature blood vessels) and CD31 revealed that SDC4 expression strongly correlated with $CD31^+/VEGFR2^{high}$ blood vessels, whereas only moderate expression was detected in $CD31^+/VEGFR2^{low}$ areas (Figure 3C and D; Figure IVC in Data Supplement). We conclude from this that, at least in the context of neovascular eye disease, SDC4 expression positively correlates with newly formed, immature blood vessels during pathological angiogenesis in both murine models and in human neovascular disease.

Angiogenic responses to VEGFA require SDC4

As the principal driver of angiogenesis in the models described above is VEGFA, we therefore wanted to explore whether responsiveness to VEGFA was a factor in the phenotypes we observed in *Sdc4-/-* animals. WT and *Sdc4-/-* mice were injected with Matrigel containing VEGFA which triggered an angiogenic response in WT mice as evidenced by plug hemoglobin content. In contrast, an angiogenic response was notably reduced in VEGFA-containing plugs from *Sdc4-/-* mice (Figure 4A and B). We next adopted a more reductive approach in which tissue explants from both choroid membranes and aortas from *Sdc4-/-, Sdc4+/-* and WT littermates were embedded in a collagen I matrix and exposed to VEGFA. In both cases, significantly more angiogenic sprouts emerged from WT, compared to *Sdc4-/-* explants (Figure 4C to E). Interestingly, explants from heterozygous (*Sdc4+/-*) mice exhibited an intermediate phenotype indicating that the angiogenic response to VEGFA associated with SDC4 is subject to gene dosage effects. WT levels of angiogenic sprouting was restored in *Sdc4-/-* null aortic rings transduced with lentiviruses to re-express full length SDC4 (Figure 4F), confirming the requirement of SDC4 for this response. Of importance, angiogenic responses to an alternative pro-angiogenic factor FGF2 were comparable between WT and *Sdc4-/-* animals, in both the Matrigel plug and the aortic ring assays (Figure VA to C in Data Supplement).

On the basis of these results, we hypothesized that endothelial SDC4 could be involved in the specific regulation of VEGFA-dependent EC responses. To this end, we analyzed EC migration by light microscopy and observed that while primary *Sdc4-/-* lung ECs were able to migrate in a growth factor-rich environment (FBS), albeit slightly less than WT ECs, their migratory response to VEGFA stimulation was negligible (Figure VD and E in Data Supplement). We further demonstrated that EC migration in response to VEGFA could be restored in *Sdc4-/-* ECs upon re-expression of full length SDC4 (Figure 4G) and, interestingly, also by a mutant form of SDC4 lacking the glycosaminoglycan chains (SDC4HA-ΔGAG), suggesting that GAG chains were not required for this function. These data suggest that the pro-angiogenic role of SDC4 in pathological neovascularization is linked to defective EC responses to VEGFA.

SDC4 resides at EC junctions and is redistributed in response to VEGFA

Previous studies have indicated that SDC4 does not impact on VEGFR2/VEGFA signaling [20]. To confirm this, we looked at VEGFR2 phosphorylation in response to VEGFA in primary lung ECs from WT and *Sdc4-/-* mice and observed no differences (Figure 5A). This was also true of the downstream signaling kinase Erk1/2 which was also phosphorylated to the same extent in WT and *Sdc4-/-* ECs in response to VEGFA (Figure 5A). We also measured cell surface expression of VEGFR2 in WT and *Sdc4-/-* cells and found this to be the same (Figure VF in Data Supplement).

In order to understand the role of SDC4 in ECs during angiogenesis, we examined its localization in HUVECs. We expressed an eGFP tagged form of SDC4 in ECs (eGFP inserted between I^{32} and D^{33} of murine SDC4 cDNA, Figure 5B), and observed a pool of SDC4-eGFP localized to EC junctions (Figure 5B, white arrows). Interestingly, stimulation of these transfected HUVECs with VEGFA led to a substantial redistribution of SDC4-eGFP (Figure 5B; Supplemental movies I and II) which was not the case in unstimulated cells. To explore this further we used fluorescence recovery after photo-bleaching (FRAP) to measure the kinetics of diffusion of SDC4-eGFP with and without VEGFA stimulation. We performed photo-bleaching of SDC4-eGFP at EC-EC contacts and observed the rate of recovery of fluorescence both under basal and VEGFA-stimulated conditions. Recovery of SDC4-eGFP fluorescence was significantly enhanced by the addition of VEGFA (Figure 5C to E), suggesting that the addition of VEGFA alters the functional status of SDC4. Previous studies have shown that phosphorylation of SDC4 at Y^{180} by Src kinase is essential for regulating the trafficking of integrins in fibroblasts[37]. To this end, we asked whether phosphorylation of this residue was important for the VEGFA stimulated response observed above with Sdc4-eGFP. We generated a mutant form of Sdc4-eGFP in which Y^{180} of SDC4 was mutated to an Alanine to make it nonphosphorylatable (SDC4(Y^{180}-A)-eGFP). Interestingly, recovery of SDC4(Y^{180}-A)-eGFP fluorescence was as rapid as SDC4-eGFP treated with VEGFA, regardless of whether they were treated with VEGFA or not (Figure 5C to E). Enhanced fluorescence recovery rates are often associated with molecules dissociating from a complex, so these results suggest that VEGFA stimulates the disassociation of SDC4 from a molecular complex at EC junctions and that this association requires SDC4 to be phosphorylated at Y^{180}. Taken together, these data indicate that not only is a pool of SDC4 resident at EC junctions, but its function is driven by VEGFA signaling.

SDC4 is required for VEGFA-induced VE-Cadherin internalization and hyper-permeability

We further explored the enrichment of SDC4 at EC cell-cell contacts, this time in untransfected cells. Here, consistent with our earlier observation in cells expressing Sdc4-eGFP, we found a pool of SDC4 at EC junctions co-localizing with both VE-Cadherin and VEGFR2 (Figure 6A). We next performed Proximity Ligation Assays (PLA) on SDC4 and VE-Cadherin and detected interactions between these two molecules under basal conditions (Figure 6B). This interaction declined after 2 and 5 mins following VEGFA treatment and recovered after 10 minutes (Figure 6C). We confirmed an interaction between SDC4 and VE-Cadherin by performing immuno-precipitation experiments with HA-tagged forms of SDC4 expressed in HUVECs. VE-Cadherin was detectable in anti-HA immuno-precipitates from cells expressing SDC4HA or SDC4HA-ΔGAG, suggesting that SDC4 GAG chains are not required for

this interaction. Interestingly, more VE-Cadherin was present in immuno-precipitates from cells expressing SDC4HA-Y^{180}-F a phosphomimetic, compared to the nonphosphorylatable form SDC4HA-Y^{180}-A (Figure VIA in Data Supplement). Furthermore, less VE-Cadherin was evident in immuno-precipitates from SDC4HA transduced cells following treatment with VEGFA (Figure VIB in Data Supplement). Collectively, this data suggests that phosphorylated SDC4 interacts with VE-Cadherin, and that treatment with VEGFA leads to dephosphorylation of SDC4 and the disruption of this interaction.

This led us to postulate that SDC4 could play a role in the regulation of VEGFA-induced VE-Cadherin internalization and tested this hypothesis in an antibody-feeding assay. We found that primary *Sdc4-/-* ECs displayed reduced VE-Cadherin internalization following exposure to VEGFA compared to WT ECs (Figure 6D and E). Additionally, cell surface biotinylation experiments revealed that whilst in WT cells biotinylated cell surface VE-Cadherin is reduced after VEGFA treatment, this was not the case with *Sdc4-/-* MLECs (Figure VIC in Data Supplement). In line with this observation, newly-formed blood vessels in retinas from *Sdc4-/-* OIR mice had fewer intracellular VE-cadherin^{+} vesicles compared to WT vasculature, whereas VE-cadherin immunostaining was more discontinuous and VE-Cadherin^{+} vesicles were more abundant (Figure VII in Data Supplement). Expression of SDC4HA, and SDC4HA-Y^{180}-F all restored VE-Cadherin internalization responses to VEGFA in Sdc4-/- MLECs, which was not the case in SDC4HA-Y^{180}-A transduced cells (Figure VIII in Data Supplement). Since VEGFA-dependent endocytosis of VE-Cadherin from the EC adherens junctions is a known to trigger of vascular permeability *in vivo* [38], we next measured the leakage of albumin-bound Evans blue from the dermal microvasculature in response to VEGFA and bradykinin (a known vasodilator) in WT and *Sdc4-/-* animals. Results showed that vascular leakage in response to VEGFA was significantly reduced in *Sdc4-/-* animals (Figure 6F and G). Together, our data identifies a novel association between SDC4 and VE-Cadherin that is modulated by VEGFA. We further reveal that SDC4 is required for VEGFA-induced VE-Cadherin internalization and hyper-permeability.

Soluble SDC4 reduces VEGFA induced VE-Cadherin internalization in a pre-clinical model of wet AMD

Lastly, we explored whether a soluble form of SDC4 (referred to as solS4, corresponding to the complete ectodomain of SDC4) could interfere with its pro-angiogenic role, in particular by disrupting the SDC4/VE-cadherin interaction. Using antibody-feeding approaches, we found that addition of solS4 to a monolayer of WT ECs prevented VEGFA-driven VE-Cadherin internalization (Figure 7A and B). Moreover, incubation of HUVECs with solS4 led to a reduction in PLA puncti between SDC4 and VE-Cadherin at EC junctions (Figure IXA in Data Supplement), indicating that it may be disrupting the SDC4/VE-Cadherin complex. In addition, solS4 treatment also abolished VEGFA-driven EC migration. This is in contrast to ECs pre-treated with soluble SDC2 (solS2), the syndecan most structurally similar to SDC4, which maintained responsiveness to VEGFA (Figure 7C). As was the case with *Sdc4-/-* primary ECs, no impact on VEGFA signaling was observed in ECs stimulated with VEGFA in the presence or absence of solS4 (Figure IXB and C in Data Supplement).We also observed reduced sprouting when aortic explants where treated with solS4 (Figure 7D and E). We next assessed whether solS4 could be

therapeutically beneficial as an anti-angiogenic compound, by testing its efficacy in the laser-induced CNV model in comparison to Aflibercept (Eylea®, Regeneron), one of the current standard therapies for neovascular AMD patients. We found that a single injection of solS4 at day 0 post-laser injury reduced the angiogenic response at day 7 by almost 50% compared to vehicle (PBS) control, achieving similar anti-angiogenic activity to that of Aflibercept (Figure 7F and G). Altogether, these results indicate that delivery of solS4 decreases VE-Cadherin internalization, EC migration and reduces pathological angiogenesis in a pre-clinical murine model of neovascular AMD.

DISCUSSION

In this work we have performed detailed analysis of both post-natal and adult micro-vasculature in *Sdc4-/-* animals and found that vascular development is not affected by genetic deletion of SDC4. However, we showed in multiple murine disease models (diabetic retinopathy, wet AMD, melanoma and epidermal carcinogenesis) that SDC4 is required for robust pathological angiogenesis. This difference can be explained by SDC4 being differentially expressed during these two chronologically-distinct processes. In fact, our data reveals that SDC4 was the only syndecan member which was upregulated in models of pathological angiogenesis and importantly, its expression correlated with immature, pathological vessels formed in the retinas of diabetic retinopathy patients. The existence of hypoxia- [39] and inflammation-related regulatory elements (i.e. NF-κB [40] within the *Sdc4* promoter region supports the concept that the expression and activity of this proteoglycan is driven by responses to hypoxia and inflammation, concomitant with pathological scenarios and important pro-angiogenic stimuli.

In the *in vivo* models described in this study, the primary driver of angiogenesis is VEGFA. We therefore explored the responses of *Sdc4-/-* cells and tissues in VEGFA stimulated angiogenesis assays (e.g. VEGFA-induced cell migration, tissue explant sprout formation) and found them to be impaired. This suggests that the defects we observed are linked to the angiogenic pathways driven by VEGFA. Importantly, normal angiogenic responses could be restored when SDC4 was expressed in *Sdc4-/-* cells and tissues. Our initial hypothesis was that SDC4 was acting as co-receptor between VEGFA and VEGFR2 through its HS chains. Recent studies suggest that this is the case for SDC4, VEGFC and VEGFR3 during pathological lymphangiogenesis [41]. However, we discounted this hypothesis since, consistent with other studies, we observed no reduction in either phosphorylation of VEGFR2 or major signaling kinases downstream of this receptor (Erk1/2) in *Sdc4-/-* ECs treated with VEGFA. These findings are in agreement with the observation that VEGFA signaling requires SDC2, not SDC4, owing to differences in the levels of 6-O-sulphation on the HS chains of these molecules [20].

An excess of SDC4 achieved either by genetic means or via exogenous addition within proteo-liposomes leads to increased angiogenesis and improved therapeutic outcomes in models of ischemic injury and myocardial infarction[23, 25, 42]. These findings support the idea that upregulation of SDC4 expression is an important component in angiogenic responses. Furthermore, silencing of SDC4 leads to an attenuation of angiogenic responses in cell-based assays [43]. Pro-angiogenic roles for SDC4 have been reported, particularly, in augmenting FGF2 signaling [23, 25, 42]. The relationship between HS and FGF2 is well established and it is likely that SDC4 HS, when in abundance in these models, is responsible for enhanced FGF2 driven cellular responses. Both 2-O and 6-O sulphated HS can promote FGF2 signaling [44-47] whereas there is a distinct requirement for 6-O sulphation on HS chains for promoting the VEGFR2/VEGFA interaction[20]. The more promiscuous HS binding requirements of FGF2 mean there is likely to be redundancy in the system and other HSPGs could be the source of the HS required to engage FGF2 in *Sdc4-/-* animals which may explain the lack of developmental angiogenic defects in these mice. In common with other studies we did not observe an effect on FGF2 induced angiogenesis in *Sdc4-/-* animals [20]. Collectively this suggests that, in the absence of

SDC4, VEGFA/VEGR2 signaling is unperturbed and this led us to speculate that SDC4 may have a role in pathological angiogenesis and is regulated by the VEGFA/VEGFR2 axis.

We demonstrated that SDC4 localizes to EC cell-cell contacts and co-localizes with the junctional protein VE-Cadherin. This is in keeping with recent proteomic studies in which SDC4 was found to be associated with EC junctional proteins [48]. EC adherens junctions are a complex assemblage of both junctional and cytoskeletal proteins and many of the molecules involved also constitute focal adhesion complexes, in which SDC4 is a known component [49]. Furthermore, numerous studies have identified roles for SDC4 in cytoskeletal rearrangements and changes in the actin cytoskeleton in a variety of cell types, including ECs [43]. The disassembly of these structures is a critical early step in angiogenesis [50] and we showed that ECs null for SDC4 exhibited defective VE-Cadherin internalization away from junctions in response to VEGFA stimulation. This was also reflected in defective vascular permeability responses *in vivo*. Our data revealed that under basal conditions SDC4 is in complex with VE-Cadherin, and this complex is disrupted rapidly following VEGFA stimulation. The presence of SDC4 in this complex is clearly an important precursor for efficient VE-Cadherin trafficking since when SDC4 is absent (e.g. in *Sdc4-/-* animals or ECs) this process was inhibited substantially. The phosphorylation status of SDC4, specifically on residue Y^{180}, is also important in regulating this process. Mutant forms of SDC4 in which this residue is mutated to Alanine did not complex effectively with VE-Cadherin and failed to restore efficient VE-Cadherin trafficking in *Sdc4-/-* ECs. Conversely, phosphomimetic mutants complexed with VE-Cadherin were capable of restoring VEGFA driven VE-Cadherin internalization. We therefore speculate that in response to VEGFA, SDC4 is dephosphorylated leading to a disruption of the SDC4/VE-Cadherin complex. Phosphorylation of this residue by c-SRC is an important control point of integrin trafficking [37] and it is not inconceivable that this may also be linked to the findings reported here, since β1 integrin activation state influences VE-cadherin localization [51, 52]. Moreover, the expression of SDC4 is required for the expression of junctional Cadherin-11 in fibroblasts [53] and in calcium signaling [54]. These studies, in conjunction with our findings suggests that SDC4 may be involved with other members of the Cadherin family in other cell types.

Our studies indicate that SDC4 is essential for efficient VE-Cadherin internalization in response to VEGFA and we show that the delivery of soluble SDC4 inhibits this process. This is in contrast other reported observations in which thrombin-cleaved fragments of both SDC3 and SDC4 extracellular core protein promote EC junctional reorganization in cultured ECs[55]. Regulatory sequences within syndecan extracellular core proteins have been identified in all 4 syndecan family members and they can impact on EC behaviour[56]. The soluble form of SDC4 used in this study comprises the entire extracellular core protein. A possible explanation for the disparity in these observations is that fragments of SDC4 ectodomain may have different properties to the full-length version. In addition, there may also be possible synergism between SDC4 and SDC3 ectodomain fragments, the full length of which can also modulate angiogenesis[57].

We also show that soluble SDC4 can reduce both VEGF-driven angiogenesis and hyper-permeability *in vivo*. Neovascularization and subsequent vascular leakage from angiogenic blood vessels is an important and exacerbating factor in neovascular eye disease [58]. Furthermore, angiogenesis blocking strategies are in

use for the treatment of a number of tumors. The most common therapeutic options involve targeting VEGFA either using antibodies or receptor-mimicking recombinant proteins. Although successful, these therapies are not without limitations, particularly with regard to patient non-response in ophthalmic indications and a significant side-effect profile when administered systemically in treating cancer [59, 60]. We demonstrate that SDC4 acts downstream of the VEGFA/VEGFR2 axis and application of a solSDC4 while disrupting the SDC4/VE-cadherin interaction has negligible impact on the phosphorylation status of key signaling kinases within ECs. Potentially therefore at least in the instances where anti-angiogenic therapies are administered systemically, fewer adverse effects might be observed in targeting SDC4/VE-Cadherin, particularly as SDC4 seems only to be upregulated on ECs during pathological scenarios. The rationale for targeting SDC4 for therapeutic benefit has been demonstrated in other disease models. Antibodies against SDC4 have been shown to block SDC4 dimerization in response to IL-1β stimulation, and these have a positive impact in models of inflammatory arthritis[61]. Furthermore, use of recombinant proteins derived from SDC4 binding partners have also proven efficacious in disease models. The Ig1 and 2 repeats from the protein tyrosine phosphatase receptor sigma (PTPRρ) have also been shown to inhibit signaling of this receptor resulting in improved outcomes in collagen-induced arthritis models[62]. Whether these reagents could be used to target pathological angiogenesis remains unexplored, but strongly support the idea that SDC4 could be targeted for therapeutic benefit in disease settings.

Taken together, our study identifies SDC4 as an essential regulatory component in VEGFA-induced VE-cadherin internalization from EC junctions during pathological angiogenesis. We believe these results provide significant further insight into the molecular events controlling neovascularization and hyper-permeability responses in diseases. The formation of abnormal blood vessels is a feature of cancer, neovascular eye diseases and chronic inflammatory conditions, which implies that SDC4 blocking strategies may have the potential to be applied in these contexts to either improve or offer a more selective alternative to existing therapies.

ACKNOWLEDGEMENTS

a) Acknowledgements: GDR, JRW, EC and TAHJ designed the experiments; GDR, JRW, EC, TAHJ, MV, HU-J interpreted the results; GDR and JRW wrote the manuscript; GDR performed choroid and aortic ring assay, matrigel plug assay, lentivirus production (JRW and SA designed and generated the cDNAs), cell migration assay, VE-Cadherin internalization assay, permeability assay, immunofluorescence staining, vascular bed staining, SDS-Page and western blotting, flow cytometry analysis; EC, GDR, SEL performed the laser induced CNV and in conjunction with MV and HU-J performed the analysis of neonatal retinal development; MV, HU-J performed the OIR experiments and analysis of human PDR membranes. MV, UM, LP and TAHJ performed two-stage carcinogenesis model and analyses. We thank Marianne Karlsberg and Terhi Tuomola for practical support.

b) Sources of funding: JRW and GDR gratefully acknowledge funding from Arthritis Research UK (Grant No. 19207 and 21177), Fight for Sight (Grant No. 1558/59), Barts and The London Charity (Grant No. MGU0313), Queen Mary Innovations, William Harvey Research Foundation, The Macular Society and the Dunhill Medical Trust (Grant No. RPGF1906\173). TAHJ, MV and HU-J gratefully acknowledge funding from the Academy of Finland, Päivikki and Sakari Sohlberg Foundation, Instrumentarium Research Foundation, Diabetes Wellness Foundation (DWF), Pirkanmaa Hospital District Research Foundation, Tampere Tuberculosis Foundation and the Finnish Cultural Foundation. JWB is a NIHR Research Professor.

c) Disclosures: The data and reagents that support the findings of this study are available from the corresponding author upon reasonable request.

REFERENCES

1. Eming SA, Martin P, Tomic-Canic M. Wound repair and regeneration: Mechanisms, signaling, and translation. *Science Translational Medicine*. 2014;6
2. Jayson GC, Kerbel R, Ellis LM, Harris AL. Antiangiogenic therapy in oncology: Current status and future directions. *Lancet*. 2016;388:518-529
3. Amadio M, Govoni S, Pascale A. Targeting vegf in eye neovascularization: What's new? A comprehensive review on current therapies and oligonucleotide-based interventions under development. *Pharmacological Research*. 2016;103:253-269
4. Carmeliet P, Jain RK. Molecular mechanisms and clinical applications of angiogenesis. *Nature*. 2011;473:298-307
5. Adams RH, Alitalo K. Molecular regulation of angiogenesis and lymphangiogenesis. *Nature reviews. Molecular cell biology*. 2007;8:464-478
6. Teleanu RI, Chircov C, Grumezescu AM, Teleanu DM. Tumor angiogenesis and anti-angiogenic strategies for cancer treatment. *Journal of clinical medicine*. 2019;9
7. Olsson AK, Dimberg A, Kreuger J, Claesson-Welsh L. Vegf receptor signalling - in control of vascular function. *Nat Rev Mol Cell Biol*. 2006;7:359-371
8. Gaengel K, Niaudet C, Hagikura K, Lavina B, Muhl L, Hofmann JJ, Ebarasi L, Nystrom S, Rymo S, Chen LL, et al.. The sphingosine-1-phosphate receptor s1pr1 restricts sprouting angiogenesis by regulating the interplay between ve-cadherin and vegfr2. *Developmental cell*. 2012;23:587-599
9. Bentley K, Franco CA, Philippides A, Blanco R, Dierkes M, Gebala V, Stanchi F, Jones M, Aspalter IM, Cagna G, et al.. The role of differential ve-cadherin dynamics in cell rearrangement during angiogenesis. *Nature cell biology*. 2014;16:309-321
10. Yamamoto H, Ehling M, Kato K, Kanai K, van Lessen M, Frye M, Zeuschner D, Nakayama M, Vestweber D, Adams RH. Integrin beta1 controls ve-cadherin localization and blood vessel stability. *Nature communications*. 2015;6:6429
11. Cao J, Ehling M, Marz S, Seebach J, Tarbashevich K, Sixta T, Pitulescu ME, Werner AC, Flach B, Montanez E, et al.. Polarized actin and ve-cadherin dynamics regulate junctional remodelling and cell migration during sprouting angiogenesis. *Nature communications*. 2017;8:2210
12. Carmeliet P, Lampugnani MG, Moons L, Breviario F, Compernolle V, Bono F, Balconi G, Spagnuolo R, Oosthuyse B, Dewerchin M, et al.. Targeted deficiency or cytosolic truncation of the ve-cadherin gene in mice impairs vegf-mediated endothelial survival and angiogenesis. *Cell*. 1999;98:147-157
13. Ashikari-Hada S, Habuchi H, Kariya Y, Kimata K. Heparin regulates vascular endothelial growth factor165-dependent mitogenic activity, tube formation, and its receptor phosphorylation of human endothelial cells. Comparison of the effects of heparin and modified heparins. *The Journal of biological chemistry*. 2005;280:31508-31515
14. Robinson CJ, Mulloy B, Gallagher JT, Stringer SE. Vegf165-binding sites within heparan sulfate encompass two highly sulfated domains and can be liberated by k5 lyase. *The Journal of biological chemistry*. 2006;281:1731-1740
15. Xie M, Li JP. Heparan sulfate proteoglycan - a common receptor for diverse cytokines. *Cellular signalling*. 2019;54:115-121
16. Alexopoulou AN, Multhaupt HA, Couchman JR. Syndecans in wound healing, inflammation and vascular biology. *The international journal of biochemistry & cell biology*. 2007;39:505-528
17. Couchman JR. Transmembrane signaling proteoglycans. *Annual review of cell and developmental biology*. 2010;26:89-114

18. Gondelaud F, Ricard-Blum S. Structures and interactions of syndecans. *The FEBS journal*. 2019;286:2994-3007
19. Afratis NA, Nikitovic D, Multhaupt HA, Theocharis AD, Couchman JR, Karamanos NK. Syndecans - key regulators of cell signaling and biological functions. *The FEBS journal*. 2017;284:27-41
20. Corti F, Wang Y, Rhodes JM, Atri D, Archer-Hartmann S, Zhang J, Zhuang ZW, Chen D, Wang T, Wang Z, et al.. N-terminal syndecan-2 domain selectively enhances 6-o heparan sulfate chains sulfation and promotes vegfa165-dependent neovascularization. *Nat Commun*. 2019;10:1562
21. Echtermeyer F, Streit M, Wilcox-Adelman S, Saoncella S, Denhez F, Detmar M, Goetinck P. Delayed wound repair and impaired angiogenesis in mice lacking syndecan-4. *The Journal of clinical investigation*. 2001;107:R9-r14
22. Ishiguro K, Kadomatsu K, Kojima T, Muramatsu H, Nakamura E, Ito M, Nagasaka T, Kobayashi H, Kusugami K, Saito H, et al.. Syndecan-4 deficiency impairs the fetal vessels in the placental labyrinth. *Dev Dyn*. 2000;219:539-544
23. Xie J, Wang J, Li R, Dai Q, Yong Y, Zong B, Xu Y, Li E, Ferro A, Xu B. Syndecan-4 over-expression preserves cardiac function in a rat model of myocardial infarction. *J Mol Cell Cardiol*. 2012;53:250-258
24. Corti F, Finetti F, Ziche M, Simons M. The syndecan-4/protein kinase cα pathway mediates prostaglandin e2-induced extracellular regulated kinase (erk) activation in endothelial cells and angiogenesis in vivo. *J Biol Chem*. 2013;288:12712-12721
25. Das S, Monteforte AJ, Singh G, Majid M, Sherman MB, Dunn AK, Baker AB. Syndecan-4 enhances therapeutic angiogenesis after hind limb ischemia in mice with type 2 diabetes. *Adv Healthc Mater*. 2016;5:1008-1013
26. Smith LE, Wesolowski E, McLellan A, Kostyk SK, D'Amato R, Sullivan R, D'Amore PA. Oxygen-induced retinopathy in the mouse. *Investigative ophthalmology & visual science*. 1994;35:101-111
27. Vähätupa M, Jääskeläinen N, Cerrada-Gimenez M, Thapa R, Järvinen T, Kalesnykas G, Uusitalo-Järvinen H. Oxygen-induced retinopathy model for ischemic retinal diseases in rodents. *J Vis Exp*. 2020
28. Stahl A, Chen J, Sapieha P, Seaward MR, Krah NM, Dennison RJ, Favazza T, Bucher F, Lofqvist C, Ong H, et al.. Postnatal weight gain modifies severity and functional outcome of oxygen-induced proliferative retinopathy. *The American journal of pathology*. 2010;177:2715-2723
29. Vahatupa M, Prince S, Vataja S, Mertimo T, Kataja M, Kinnunen K, Marjomaki V, Uusitalo H, Komatsu M, Jarvinen TA, Uusitalo-Jarvinen H. Lack of r-ras leads to increased vascular permeability in ischemic retinopathy. *Investigative ophthalmology & visual science*. 2016;57:4898-4909
30. Filler RB, Roberts SJ, Girardi M. Cutaneous two-stage chemical carcinogenesis. *CSH Protoc*. 2007;2007:pdb.prot4837
31. May U, Prince S, Vahatupa M, Laitinen AM, Nieminen K, Uusitalo-Jarvinen H, Jarvinen TA. Resistance of r-ras knockout mice to skin tumour induction. *Scientific reports*. 2015;5:11663
32. Vahatupa M, Pemmari T, Junttila I, Pesu M, Jarvinen TAH. Chemical-induced skin carcinogenesis model using dimethylbenz[a]anthracene and 12-o-tetradecanoyl phorbol-13-acetate (dmba-tpa). *Journal of visualized experiments : JoVE*. 2019
33. Vähätupa M, Järvinen TAH, Uusitalo-Järvinen H. Exploration of oxygen-induced retinopathy model to discover new therapeutic drug targets in retinopathies. *Front Pharmacol*. 2020;11:873

34. Grossniklaus HE, Kang SJ, Berglin L. Animal models of choroidal and retinal neovascularization. *Progress in Retinal and Eye Research*. 2010;29:500-519
35. Perez-Losada J, Balmain A. Stem-cell hierarchy in skin cancer. *Nature reviews. Cancer*. 2003;3:434-443
36. Arokiasamy S, Balderstone MJM, De Rossi G, Whiteford JR. Syndecan-3 in inflammation and angiogenesis. *Front Immunol*. 2019;10:3031
37. Morgan MR, Hamidi H, Bass MD, Warwood S, Ballestrem C, Humphries MJ. Syndecan-4 phosphorylation is a control point for integrin recycling. *Dev Cell*. 2013;24:472-485
38. Gavard J, Gutkind JS. Vegf controls endothelial-cell permeability by promoting the beta-arrestin-dependent endocytosis of ve-cadherin. *Nature cell biology*. 2006;8:1223-1234
39. Fujita N, Hirose Y, Tran CM, Chiba K, Miyamoto T, Toyama Y, Shapiro IM, Risbud MV. Hif-1-phd2 axis controls expression of syndecan 4 in nucleus pulposus cells. *FASEB journal : official publication of the Federation of American Societies for Experimental Biology*. 2014;28:2455-2465
40. Okuyama E, Suzuki A, Murata M, Ando Y, Kato I, Takagi Y, Takagi A, Murate T, Saito H, Kojima T. Molecular mechanisms of syndecan-4 upregulation by tnf-alpha in the endothelium-like eahy926 cells. *Journal of biochemistry*. 2013;154:41-50
41. Johns SC, Yin X, Jeltsch M, Bishop JR, Schuksz M, El Ghazal R, Wilcox-Adelman SA, Alitalo K, Fuster MM. Functional importance of a proteoglycan coreceptor in pathologic lymphangiogenesis. *Circulation research*. 2016;119:210-221
42. Jang E, Albadawi H, Watkins MT, Edelman ER, Baker AB. Syndecan-4 proteoliposomes enhance fibroblast growth factor-2 (fgf-2)-induced proliferation, migration, and neovascularization of ischemic muscle. *Proc Natl Acad Sci U S A*. 2012;109:1679-1684
43. Cavalheiro RP, Lima MA, Jarrouge-Bouças TR, Viana GM, Lopes CC, Coulson-Thomas VJ, Dreyfuss JL, Yates EA, Tersariol ILS, et al.. Coupling of vinculin to f-actin demands syndecan-4 proteoglycan. *Matrix Biol*. 2017;63:23-37
44. Kariya Y, Kyogashima M, Suzuki K, Isomura T, Sakamoto T, Horie K, Ishihara M, Takano R, Kamei K, Hara S. Preparation of completely 6-o-desulfated heparin and its ability to enhance activity of basic fibroblast growth factor. *J Biol Chem*. 2000;275:25949-25958
45. Pye DA, Vives RR, Turnbull JE, Hyde P, Gallagher JT. Heparan sulfate oligosaccharides require 6-o-sulfation for promotion of basic fibroblast growth factor mitogenic activity. *J Biol Chem*. 1998;273:22936-22942
46. Maccarana M, Casu B, Lindahl U. Minimal sequence in heparin/heparan sulfate required for binding of basic fibroblast growth factor. *J Biol Chem*. 1993;268:23898-23905
47. Jastrebova N, Vanwildemeersch M, Lindahl U, Spillmann D. Heparan sulfate domain organization and sulfation modulate fgf-induced cell signaling. *J Biol Chem*. 2010;285:26842-26851
48. Kostelnik KB, Barker A, Schultz C, Mitchell TP, Rajeeve V, White IJ, Aurrand-Lions M, Nourshargh S, Cutillas P, Nightingale TD. Dynamic trafficking and turnover of jam-c is essential for endothelial cell migration. *PLoS biology*. 2019;17:e3000554
49. Woods A, Couchman JR. Syndecan 4 heparan sulfate proteoglycan is a selectively enriched and widespread focal adhesion component. *Mol Biol Cell*. 1994;5:183-192
50. Dejana E, Giampietro C. Vascular endothelial-cadherin and vascular stability. *Current opinion in hematology*. 2012;19:218-223

51. Pulous FE, Grimsley-Myers CM, Kansal S, Kowalczyk AP, Petrich BG. Talin-dependent integrin activation regulates ve-cadherin localization and endothelial cell barrier function. *Circulation research*. 2019;124:891-903
52. Hakanpaa L, Kiss EA, Jacquemet G, Miinalainen I, Lerche M, Guzmán C, Mervaala E, Eklund L, Ivaska J, Saharinen P. Targeting β1-integrin inhibits vascular leakage in endotoxemia. *Proc Natl Acad Sci U S A*. 2018;115:E6467-e6476
53. Gopal S, Multhaupt HAB, Pocock R, Couchman JR. Cell-extracellular matrix and cell-cell adhesion are linked by syndecan-4. *Matrix Biol*. 2017;60-61:57-69
54. Gopal S, Sogaard P, Multhaupt HA, Pataki C, Okina E, Xian X, Pedersen ME, Stevens T, Griesbeck O, Park PW, Pocock R, Couchman JR. Transmembrane proteoglycans control stretch-activated channels to set cytosolic calcium levels. *The Journal of cell biology*. 2015;210:1199-1211
55. Jannaway M, Yang XY, Meegan JE, Coleman DC, Yuari SY. Thrombin-cleaved syndecan-3/-4 ectodomain fragments mediate endothelial barrier dysfunction. *Plos One*. 2019;14
56. De Rossi G, Whiteford JR. Novel insight into the biological functions of syndecan ectodomain core proteins. *Biofactors*. 2013;39:374-382
57. De Rossi G, Whiteford JR. A novel role for syndecan-3 in angiogenesis. *F1000Res*. 2013;2:270
58. Soubrane G. Macular edema of choroidal origin. *Developments in ophthalmology*. 2017;58:202-219
59. Sadda SR, Guymer R, Mones JM, Tufail A, Jaffe GJ. Anti-vascular endothelial growth factor use and atrophy in neovascular age-related macular degeneration: Systematic literature review and expert opinion. *Ophthalmology*. 2019
60. Jaszai J, Schmidt MHH. Trends and challenges in tumor anti-angiogenic therapies. *Cells*. 2019;8
61. Godmann L, Bollmann M, Korb-Pap A, Konig U, Sherwood J, Beckmann D, Muhlenberg K, Echtermeyer F, Whiteford J, De Rossi G, et al.. Antibody-mediated inhibition of syndecan-4 dimerisation reduces interleukin (il)-1 receptor trafficking and signalling. *Ann. Rheum. Dis.* 2020;79:481-489
62. Doody KM, Stanford SM, Sacchetti C, Svensson MND, Coles C, Mitakidis N, Kiosses WB, Bartok B, Fos C, Cory E, Sah RL, et al.. Targeting phosphatase-dependent proteoglycan switch for rheumatoid arthritis therapy. *Sci. Transl. Med.* 2015;7:12

HIGHLIGHTS

- Syndecan-4 null mice are protected in models of neovascular eye diseases and skin tumor models due to defective angiogenesis.

- Syndecan-4 expression is upregulated during pathological angiogenesis in mice and is selectively enriched in immature blood vessels in the retinas of diabetic retinopathy patients.

- A pool of Syndecan-4 resides at endothelial cell junctions, and has no role in VEGFA/VEGFR2 signaling, but rather, is downstream of this interaction.

- Syndecan-4 null animals and cells show inefficient VEGFA-induced VE-Cadherin internalization and this is reflected *in vivo* by aberrant vascular permeability responses to VEGFA.

Figures

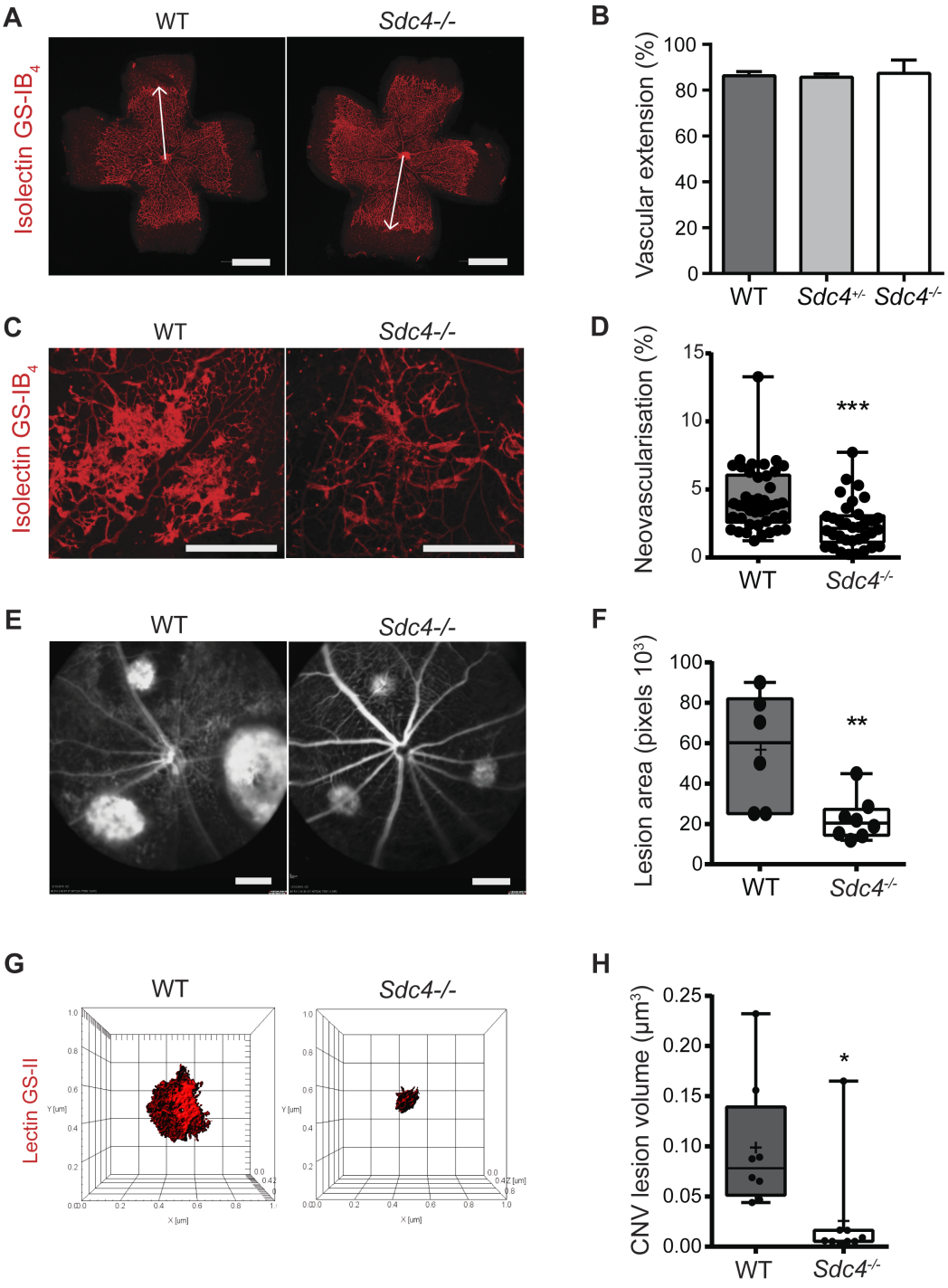

Figure 1. Pathological angiogenesis in murine models of neovascular eye disease requires SDC4.

Developmental retinal angiogenesis in *Sdc4-/-* mice proceeds at the same rate as WT. **A,** Micrographs comparing retinal micro-vessel formation between *Sdc4-/-* and WT p6 neonates (Scale bar, 1 mm). **B**, Retinas were stained with isolectin GS-IB4, and the distance between the optical nerve and the angiogenic front (arrows) was measured and the extent of retinal angiogenesis between WT, *Sdc4+/-* and *Sdc4-/-*

p6 neonates compared (n=10-15 animals/genotype). **C,** Neovascular tuft formation in response to OIR is reduced in *Sdc4-/-* p17 neonates. Representative micrographs of retinas stained with isolectin GS-IB4 (scale bar = 500µm). **D,** Quantification of neovascular tufts (~40 eyes/group). **E,** Micrographs showing *Sdc4-/-* animals exhibit less angiogenesis in the laser induced CNV model as evident from reduced lesion area (n=6-8 animals/group, Scale bar = 2.4 mm). **F,** Densitometry measurements of CNV lesions comparing responses between WT and *Sdc4-/-* animals. **G,** Staining of CNV lesions with lectin GS-II followed by 3D confocal reconstruction. **H,** CNV lesion volume was calculated using Imaris Bitplane software on the basis of lectin GS-II staining. n=5-6 animals for each group. Centre line, median. Plus sign, mean. Error bars indicate min and max values. *P < 0.05; **P < 0.01; ***P<0.001.

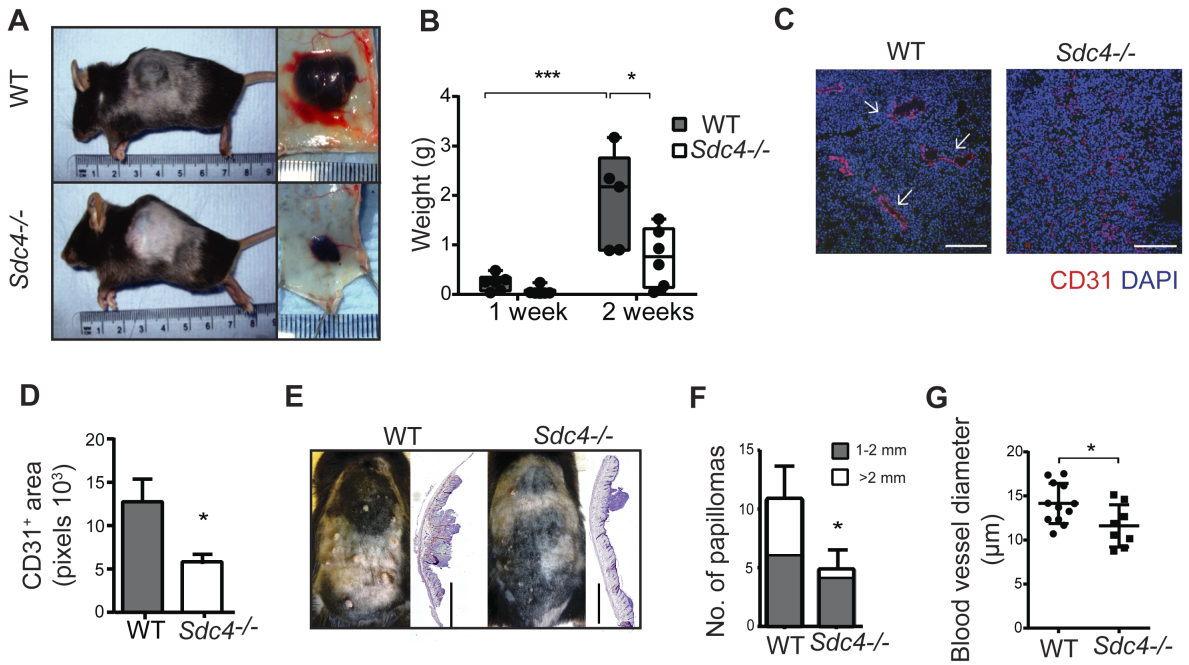

Figure 2. Tumor angiogenesis is impaired in *Sdc4-/-* animals.

A, Micrographs of B16F1 melanomas from WT and *Sdc4-/-* animals showing reduced tumor volume as quantified in **B,** (n=5-6 mice/group). **C,** Tumor vessels (arrowheads) appear in WT sections but are not obvious in B16F1 melanomas from *Sdc4-/-* mice (Ki-67, blue; CD31 red, scale bar, 100 µm), **D,** quantification of tumor vessel coverage (n=5/group, 3 images/animal). **E,** Papilloma formation is reduced in *Sdc4-/-* mice in the DBMA/TPA model. Micrographs of animals (left) and sections of skin (right, H&E stained) from WT and *Sdc4-/-* animals at week 19 (scale bar, 2 mm). **F,** Reduced size of papillomas at end of the experiment (n=7 mice/group). **G,** Tumor sections from WT and *Sdc4-/-* animals were immuno-stained for the EC marker CD31and vessel width was measured. *P < 0.05; ***P < 0.001.

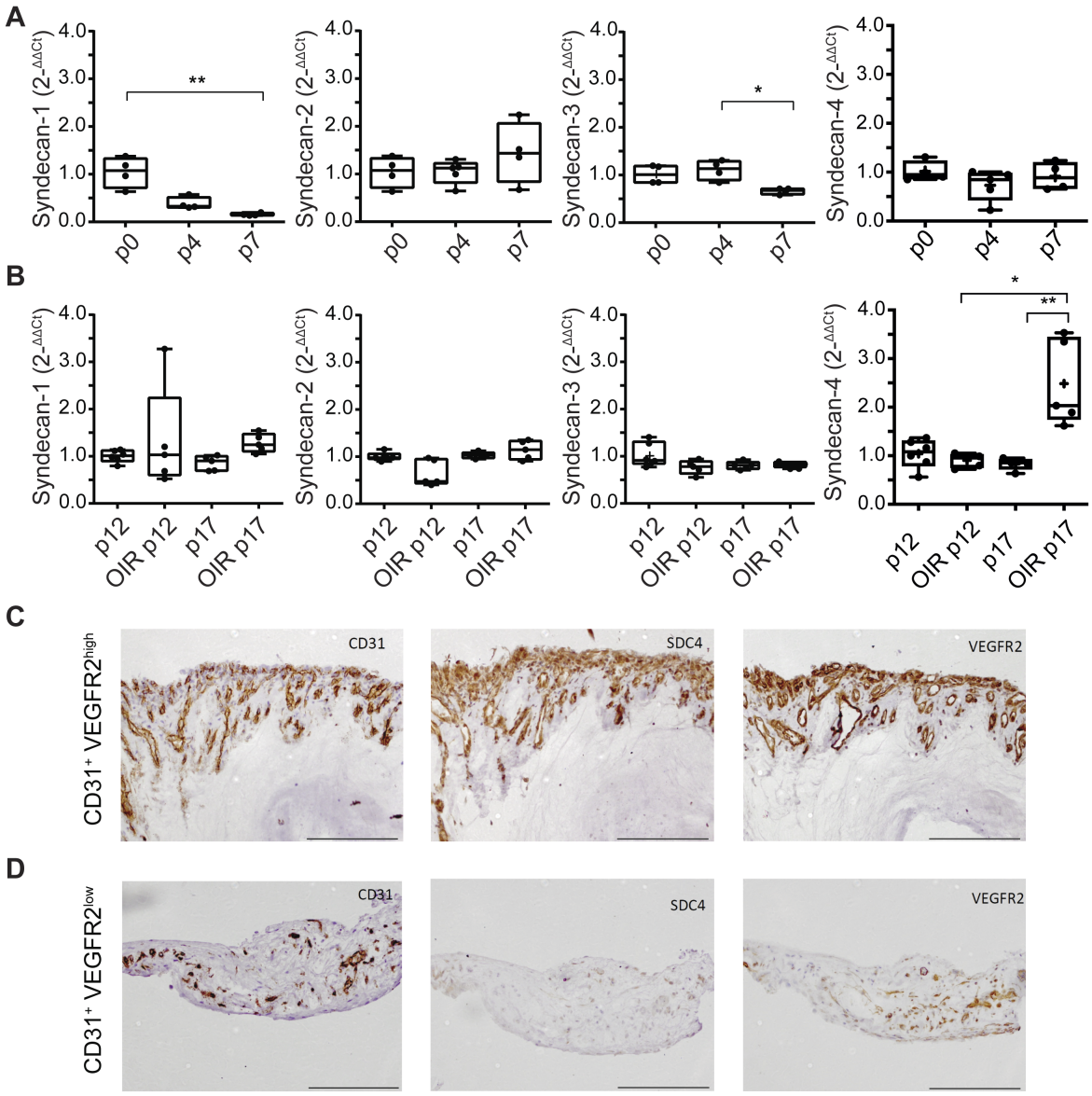

Figure 3. SDC4 expression is upregulated during pathological angiogenesis.

A, Syndecan gene expression profile during early stages of murine retinal angiogenesis. Eyes were enucleated on postnatal day 0, 4 and 7, mRNA extracted and quantified by qPCR. **B,** Syndecan gene expression in neonates subjected to OIR (P12 vaso-obliteration phase, P17 angiogenic phase) and in untreated controls. Centre line, median. Plus sign, mean. N=4-6 animals for each group. Error bars indicate min and max values. *P < 0.05; **P < 0.01. (**C**, and **D**,) Consecutive sections of human proliferative diabetic retinopathy membrane stained for CD31 marker of blood vessels), VEGFR2 (marker of new immature vessels), and SDC4. Regions of high VEGFR2 expression on ECs have correspondingly high levels of Sdc4 expression **C,** and this is not the case on sections where there is low VEGFR2 expression **D,**. Scale bar, 200 µm. Images are representative of n=6 patients.

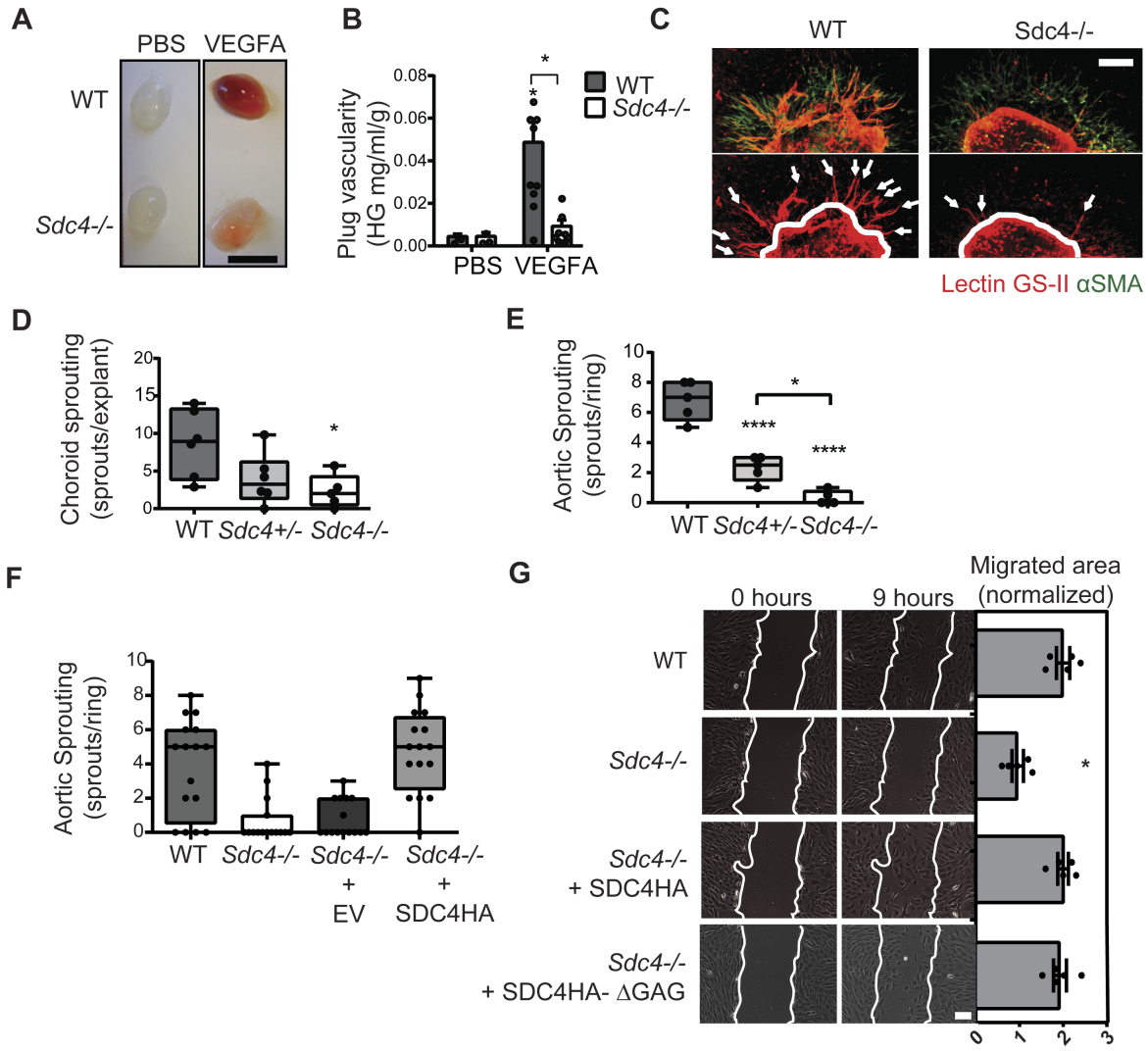

Figure 4. Functional angiogenic responses to VEGFA are impaired in *Sdc4-/-* explants and ECs.

A, Matrigel supplemented with PBS or VEGFA (50 ng) was injected subcutaneously in the flank of WT or *Sdc4-/-* mice. Images are representative of plugs extracted 7 days post-injection. Scale bar, 1 cm. **B,** Plug vascularity was expressed as the amount of haemoglobin released from the plugs per ml of Matrigel and normalized for the plug weight. n=5-6 animal for each group (2 plugs per animal). **C,** Fragments (1 mm^2) of choroid were dissected from adult WT, *Sdc4+/-* and *Sdc4-/-* littermates and cultured as explants in VEGFA-containing medium. Explants were stained with lectin GS-II (red) and anti-αSMA (green) after 7 days in culture and imaged using a Zeiss LSM 800 confocal laser scanning microscope with a 10x objective. Arrows show angiogenic sprouts. Scale bar, 100 μM. **D,** Sprouting was quantified by manually counting the number of sprouts per explant. n=5-6 animal for each group, 10 explants per animal. **E,** Quantification of sprout formation from aortic ring explants (n=5-6 animal for each group, 15-20 rings per animal). **F,** *Sdc4-/-* aortic rings were lentivirally transduced to express either eGFP (EV) or SDC4 (SDC4), n=3 animals per group, 5-6 explants per animal. **G,** *Sdc4-/-* MLECs were lentivirally transduced to

express either SDC4 or SDC4ΔGAG, and the migration of these cells compared to WT and *Sdc4-/-* in scratch wound migration assays. Cells were serum starved prior to the addition of VEGFA (10 ng/ml) and images at 0 hours and 9 hours are shown. Scale bar, 200 µm. Migrated area was calculated by subtracting the final scratch area from the initial scratch area using ImageJ. n=3-4, *p<0.05, **p<0.01, ****p<0.0001.

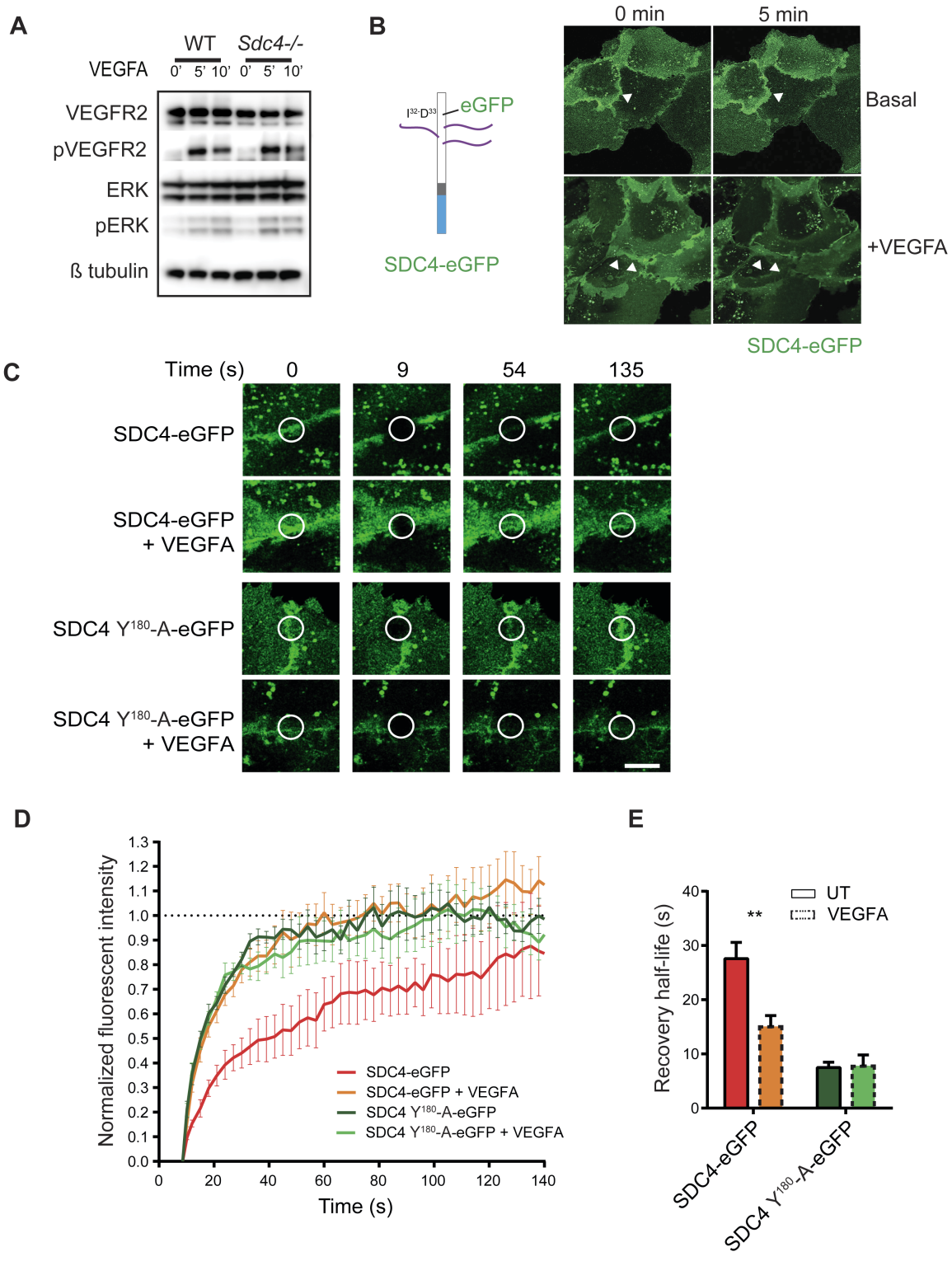

Figure 5. SDC4 acts down stream of VEGFA/VEGFR2 signaling.

A, Western blots of either WT or *Sdc4-/-* MLEC lysates harvested at different time points after VEGFA stimulation. Levels of phoshpo-VEGR2 and Erk1/2 were assayed. **B,** The complete coding sequence of eGFP was inserted into murine SDC4 between I^{32} and D^{33} and cloned into lentiviral expression vectors (diagram). Fluorescence confocal images of transfected HUVECS showing SDC4-eGFP localizes to EC junctions, and this is altered by VEGFA stimulation. Images correspond to the first and last of a 5 minute time lapse video (see Supplemental Movies 1 and 2). Cells were stimulated as indicated. **C,** Confocal images of FRAP of HUVECs expressing SDC4-eGFP or SDC4 Y180-A-eGFP at the time points indicated in the presence or absence of VEGFA stimulation. FRAP and image capture were performed using a Zeiss LSM 800 confocal laser scanning microscope with a 63x objective. **D,** Quantification of fluorescence recovery of Sdc4-eGFP and **E,** plots of the half-life of recovery for each of the treatments. n=3, **p<0.01.

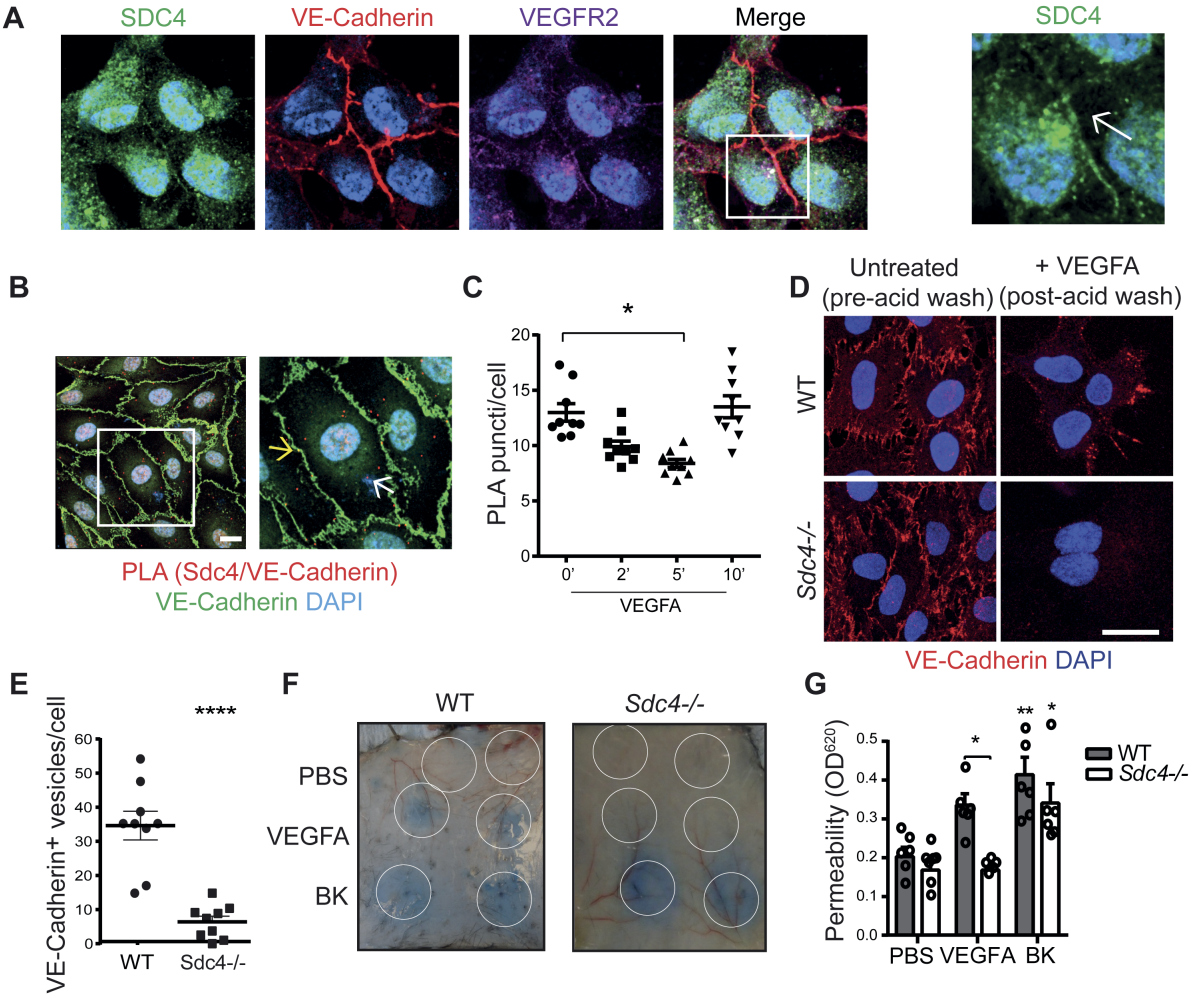

Figure 6. SDC4 is required for efficient VE-Cadherin redistribution at EC junctions in response to VEGFA.

A, Immunofluorescence staining for endogenous SDC4 (green) shows co-localization with VE-Cadherin (red) and VEGFR2 (purple) at EC junctions. Scale bar,

20 µm. **B,** Confocal micrographs of HUVECs showing proximity ligation puncti on the cell surface (red dots) between SDC4 and VE-Cadherin (nuclei, blue; VE-Cadherin, green). An example of junctional punctum (yellow arrow) and a non-junctional punctum (white arrow) is shown on the right hand micrograph. Scale bar, 10 µm. **C,** Quantification of SDC4/VE-Cadherin PLA puncta on the cell surface over time after VEGFA stimulation (10ng/ml). **D,** MLECs from WT and *Sdc4-/-* mice were washed with PBS and incubated with anti-VE-Cadherin antibody at 4 °C for 1 hour. Unbound antibody was washed away and cells stimulated with VEGFA (30 ng/ml) for 10 min at 37 °C to promote VE-Cadherin internalization. Cells were then subjected to an acid wash to remove cell surface antibody. VE-Cadherin (red), DAPI (blue). Scale bar, 20 µm. **E,** Images of MLECs treated with VEGFA and acid-washed were analyzed on Imaris software and VE-cadherin+ vesicles were counted and divided by the number of nuclei in the field of view. n=3. Images are representative of one experiment where 9 images per condition were analyzed **F,** Evans blue was injected into the tail vein of WT and *Sdc4-/-* mice, followed by subcutaneous injections of PBS, VEGFA (100 ng) or Bradykinin (BK, 100 µg). Images show the local extravasation of the dye from underneath the skin 90 minutes post-injection, white circles indicate the approximate injection area. **G,** Skin punches corresponding to the injection sites were collected and Evans blue extracted in formamide overnight. Permeability was quantified by measuring the optical density at 620 nm of the skin extracts and values were normalized on the basis of tissue weight. n=6-8 animals per condition. Data are mean ± s.e.m. *P < 0.05; **P < 0.01; ****P<0.0001. Statistical comparisons were made between PBS and treatments within the same genotype unless otherwise indicated.

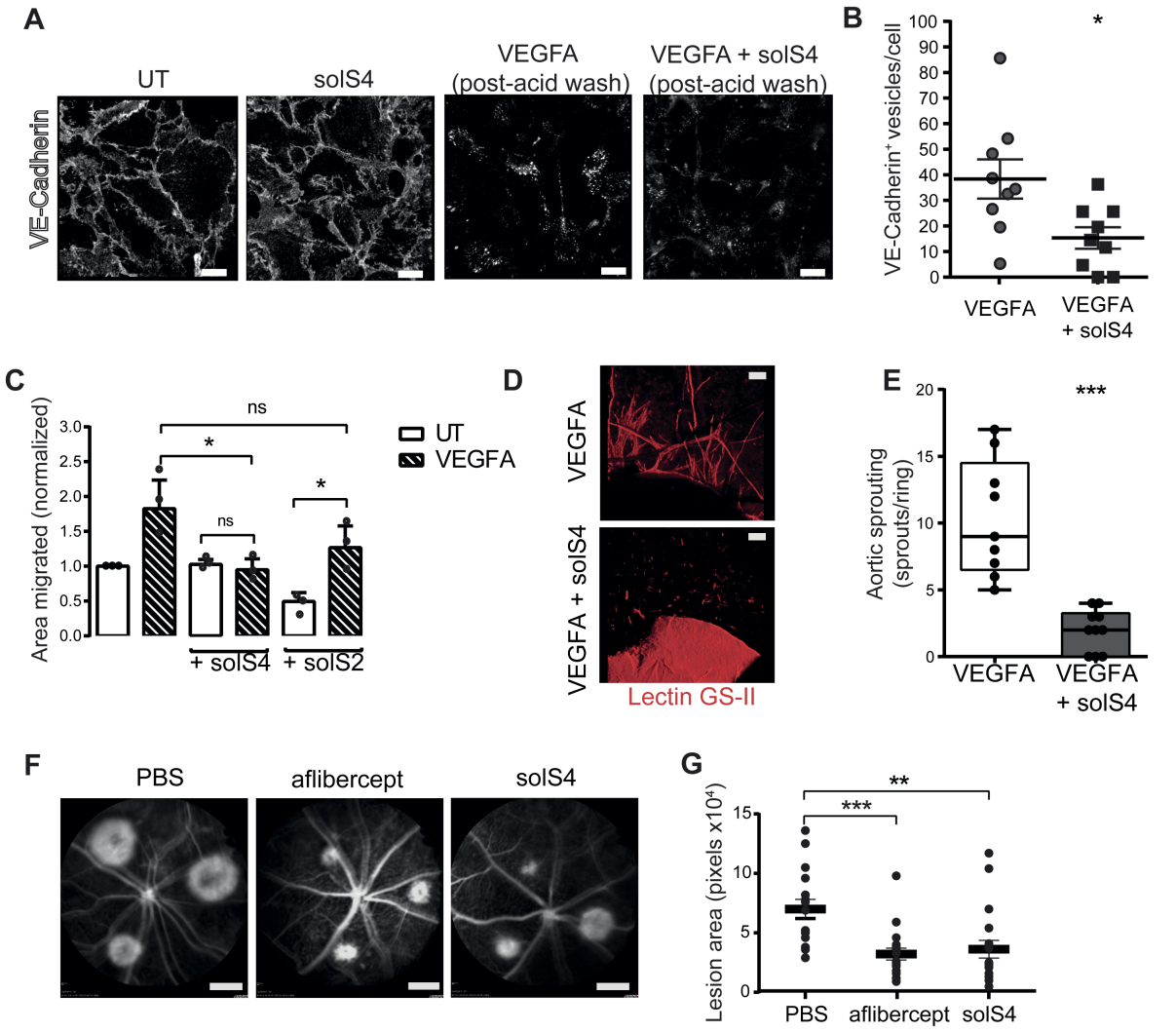

Figure 7. The extracellular core protein of SDC4 (solS4) inhibits VEGFA induced VE Cadherin internalization in vitro and choroidal neovascularization *in vivo*.

A, Confocal images of VE-Cadherin antibody 'washout' experiments. WT MLECs were washed with PBS and incubated with anti-VE-Cadherin antibody at 4 °C for 1 hour. Unbound antibody was washed away and cells stimulated with VEGFA (30 ng/ml) for 10 min with or without SolS4 (3.5 nM) at 37 °C to promote VE-Cadherin internalization followed by acid washing. VE-Cadherin (white). Scale bar, 20 μm. **B.** Images of MLECs treated with VEGFA and acid-washed were analyzed on Imaris software and VE-cadherin+ vesicles were counted and divided by the number of nuclei in the field of view. 9 images per condition were analyzed. n=3 Scale bar, 20 μm. **C.** HUVECs were scratched and incubated in serum-free media with or without VEGFA (20 ng/ml) and with or without SolS4 or solS2 (3.5 nM) for 16 hours. Migrated area was calculated by subtracting the final scratch area to the initial scratch area using ImageJ. n=3. **D,** Micrographs of C57BL6 murine aortic rings embedded in Collagen I and cultured as explants in VEGFA-containing medium with or without solS4 (3.5 nM) for 7 days. **E,** Manual quantification of angiogenic sprouts. (n=4, 5-15 rings/condition). Scale bar, 10 μm. **F,** Fundus fluorescein angiograms of

WT animals at day 7 post laser induced CNV. Intravitreal injection of 1 µl of either PBS, Aflibercept (10 µg) or solS4 (100 ng) were performed at day 0 directly after laser burns were applied. Scale bar, 2.4 mm. **G,** The CNV lesion areas were quantified using ImageJ, each dot represents the average of 3 lesions per eye. n=7-9 animals per condition. Data are means and error bars indicate SEM in B, C and G and min and max values in E. *P < 0.05; **P < 0.01; ***P<0.001.

SUPPLEMENTAL MATERIAL

- Supplemental figures and figures legends
- Supplemental material and methods
- Major resources table

Pathological angiogenesis requires Syndecan-4 for efficient VEGFA-induced VE-Cadherin internalization

Giulia De Rossi[1,5]*, Maria Vähätupa[2], Enrico Cristante[3], Samantha Arokiasamy[1], Sidath E. Liyanage[3], Ulrike May[2], Laura Pellinen[2], Hannele Uusitalo-Järvinen[2], James W. Bainbridge[3,4], Tero A.H. Järvinen[2] and James R. Whiteford[1]*.

Affiliations: [1]William Harvey Research Institute, Barts and The London School of Medicine and Dentistry, Queen Mary University of London, Charterhouse Square, London EC1M 6BQ, United Kingdom.

[2]Faculty of Medicine & Health Technology, Tampere University, 33014 Tampere, Finland & Departments of Orthopedics & Traumatology and Tampere Eye Centre, Tampere University Hospital, 33521 Tampere, Finland.

[3]UCL Institute of Ophthalmology, Genetics department, 11-43 Bath Street, London EC1V 9EL, UK.

[4]NIHR Biomedical Research Centre at Moorfields Eye Hospital NHS Foundation Trust, City Road, London EC1V 2PD, UK.

[5]UCL Institute of Ophthalmology, Department of Cell Biology, 11-43 Bath Street, London EC1V 9EL, UK.

Running title: VE-Cadherin and Syndecan-4 in Angiogenesis

Corresponding authors:

JRW, j.whiteford@qmul.ac.uk , William Harvey Research Institute, Queen Mary University of London, Charterhouse Square, London EC1M 6BQ, UK. Tel: +44(0)2078823909;

GDR, giulia.derossi@ucl.ac.uk , UCL Institute of Ophthalmology, Department of Cell Biology, 11-43 Bath Street, London EC1V 9EL, UK. Tel: +44(0)2076084016

SUPPLEMENTAL FIGURES

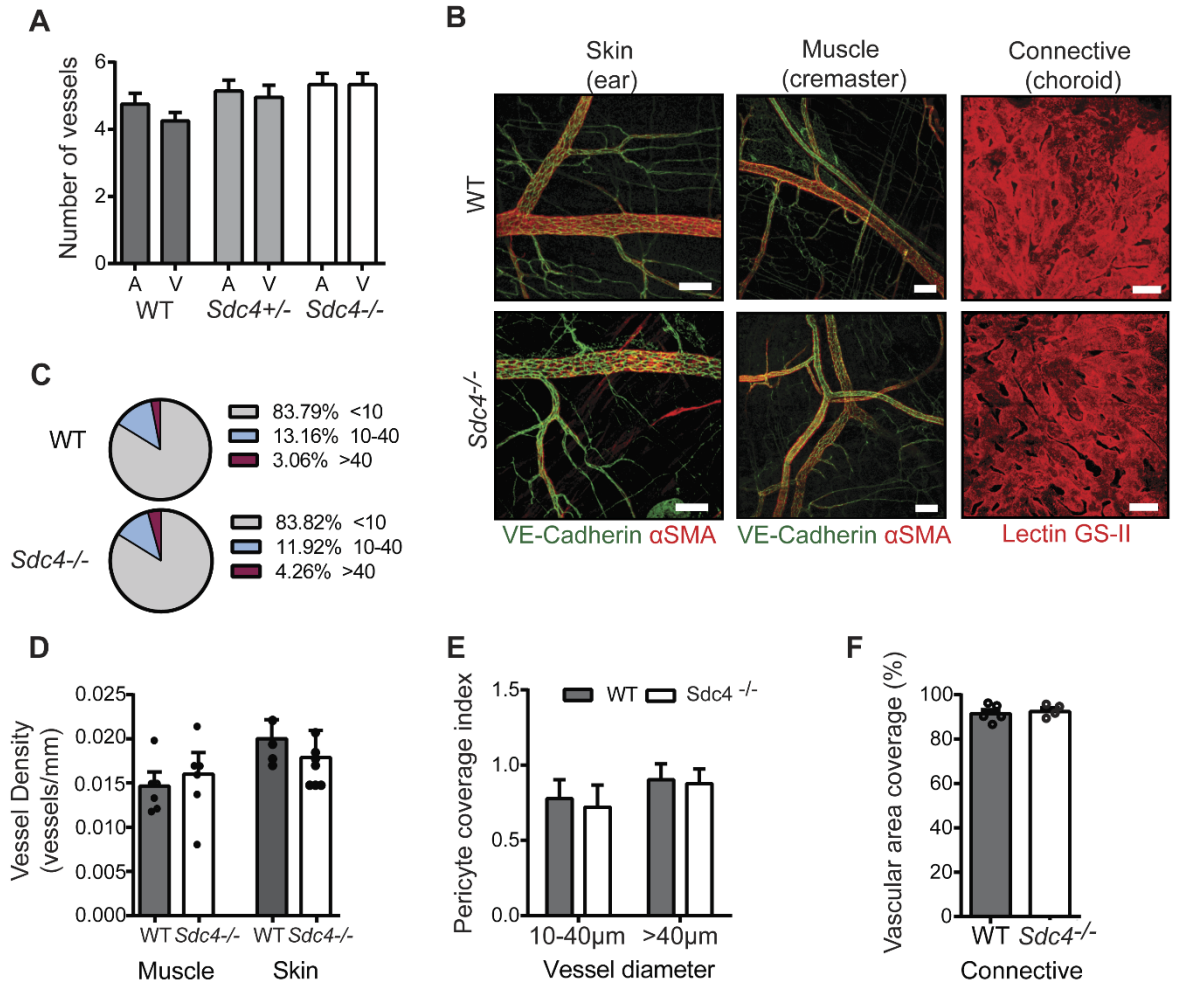

Figure I. Vascular development in *Sdc4-/-* mice in comparable to WT. A, The number of arteries and veins in P6 WT, *Sdc4+/-* and *Sdc4-/-* neonate retinas was calculated on the basis of the αSMA staining (αSMA+ artery, αSMA- vein) and showed no significant differences (n=10-15 animals per genotype). **B,** Representative images of the adult vasculature in the skin, cremaster muscle and choroid of WT and *Sdc4-/-* animals. Skin and muscle tissues were stained with VE-Cadherin (green) and αSMA (red). Scale bar, 100 μm. Choroid was stained with Lectin GS-II (red). Scale bar, 20 μm. **C,** Distribution of large (more than 40 μm in diameter), intermediate (between 10 and 40 μm in diameter) and small (less than 10 μm in diameter) vessels in the skin of WT and *Sdc4-/-* animals. **D,** Quantification of vascularity expressed as the average number of vessels crossing an arbitrary line. **E,** Pericyte coverage index was expressed as the percentage of vessel area covered by αSMA in both venules (10<40 μm) and veins (>40 μm) using ImageJ. **F,** Choroidal vascular area coverage was expressed as the percentage of the field of view covered by lectin GS-II area. n=5 animals per group, 10 images per animal.

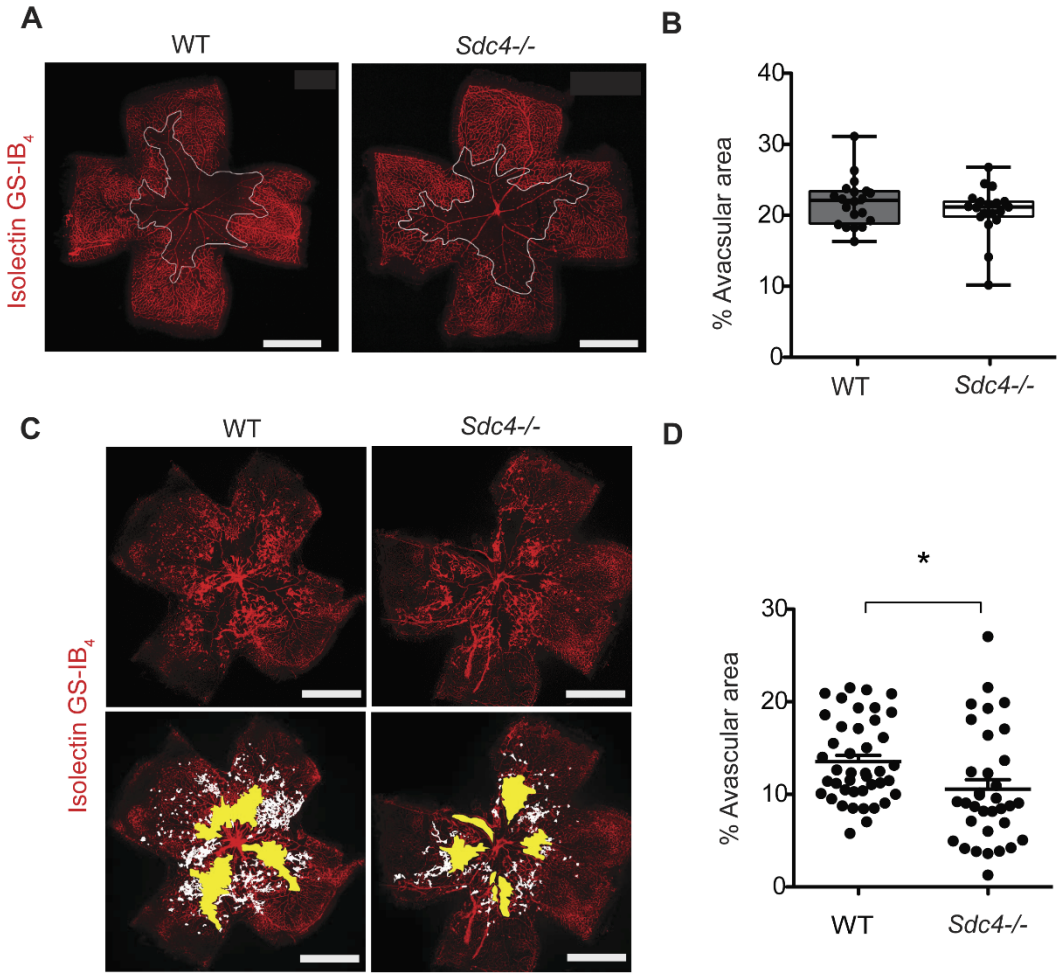

Figure II. *Sdc4-/-* response to hyperoxia is comparable to WT. A, Whole-mount retinal vasculature stained with isolectin GS-IB4 (red) harvested from WT and *Sdc4-/-* mice at P12 (vascular regression phase) of OIR, avascular regions are indicated by a white boundary line. Scale bar, 500 µm. **B,** Vascular obliteration is expressed as the percentage of retina occupied by avascular area. **C,** Whole-mount retinal vasculature stained with isolectin GS-IB4 (red) harvested from WT and *Sdc4-/-* mice at P17 of OIR. Avascular area (yellow) and neovascular tufts (white). Scale bar, 500 µm. **D,** Physiological revascularization is expressed as the percentage of total retinal area still avascular. n=3, total retinas analysed 42 WT, 34 *Sdc4-/-*. *P < 0.05.

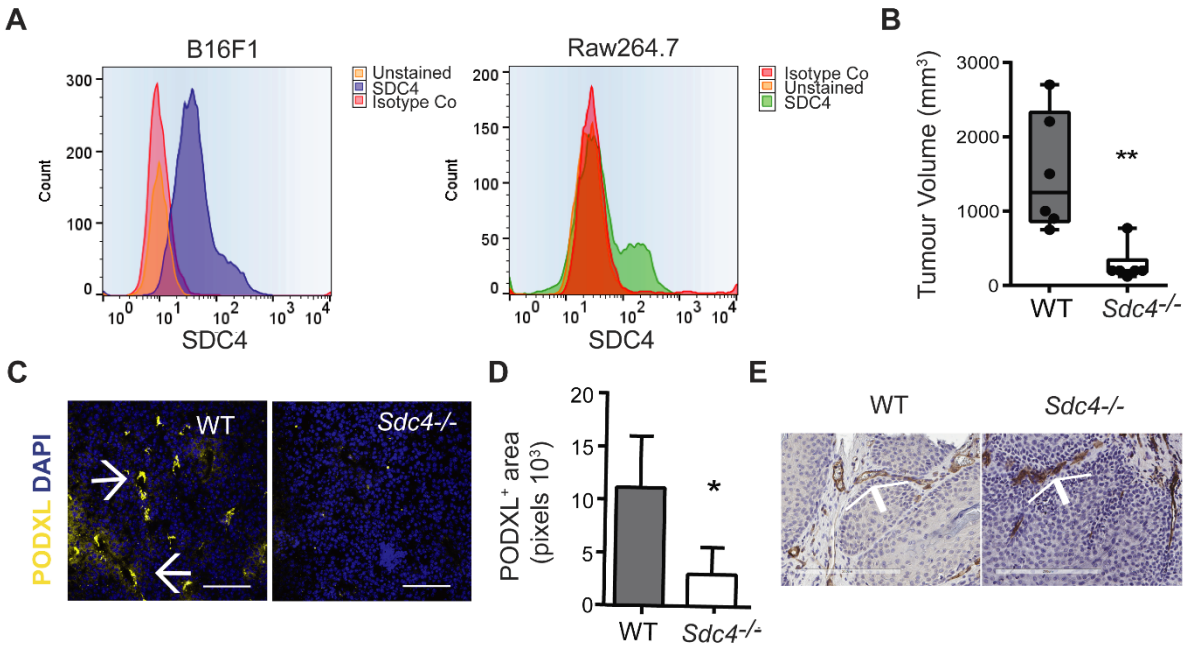

Figure III. B16F1 melanoma cells express SDC4. A, Flow cytometry analysis of B16F1 cells show SDC4 is expressed on the cell surface. As a control Raw246.7 macrophages which express low levels of SDC4 were used. **B,** B16F1 tumour volume is reduced in *Sdc4-/-* mice after 1 week (n=5-6 per group). **C,** Tumor vessels (arrowheads) appear in WT sections but are not obvious in B16F1 melanomas from *Sdc4-/-* mice (DAPI, blue; Podocalyxin yellow, scale bar, 100 μm), **D,** quantification of tumor vessel coverage (n=5/group, 3 images/animal). **E,** Sections from DMBA/TPA papilloma sections from WT and *Sdc4-/-* animals immuno-stained for the EC marker CD31 (vessels are indicated by arrow head, scale bar, 100 μm).

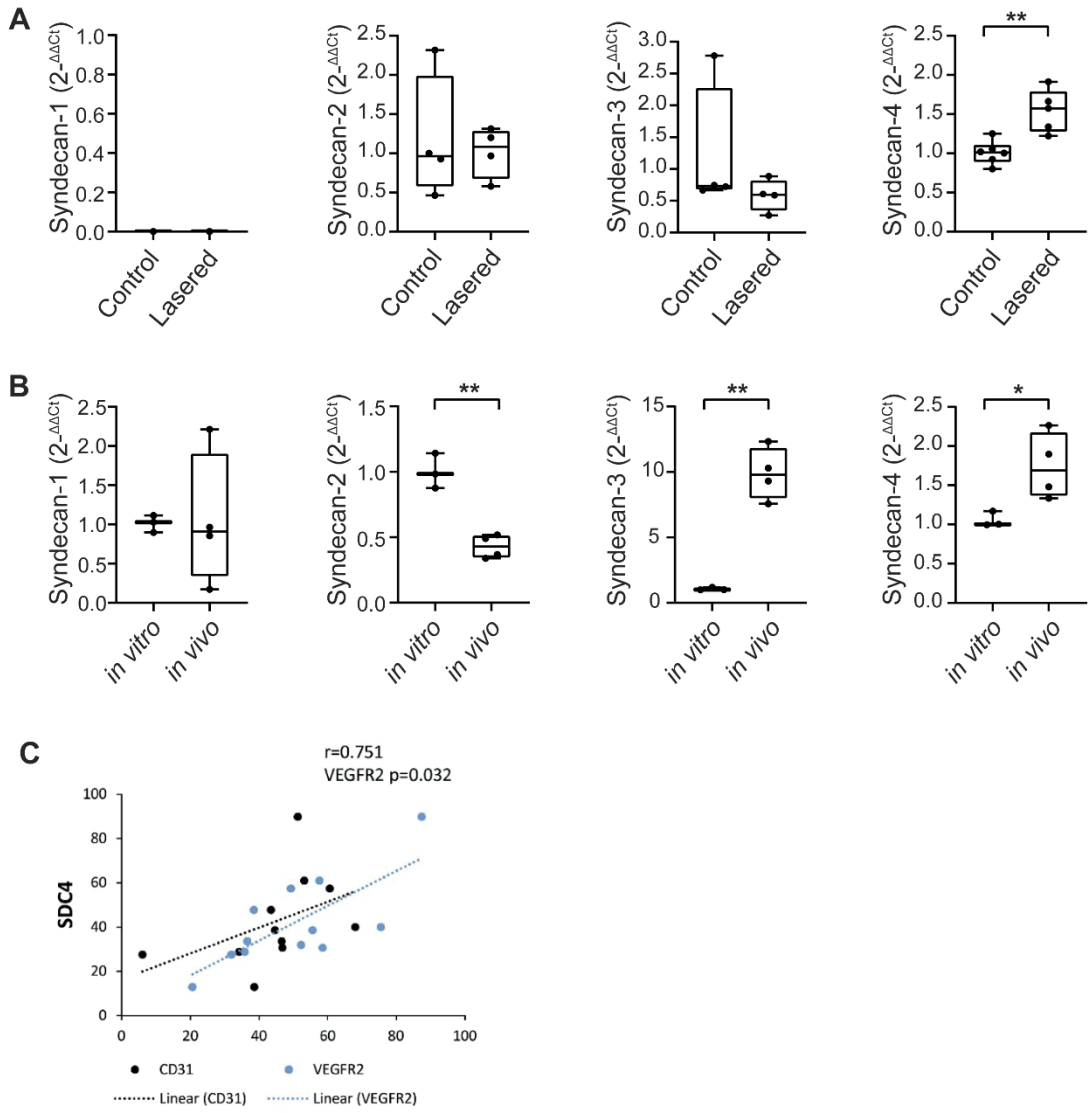

Figure IV. SDC4 expression is upregulated in response to laser induced CNV and in B16F1 melanomas. A, Syndecan gene expression in retinas from control and laser induced CNV animals (7 days post injury, n=4 animals). **B,** Syndecan gene expression in cultured B16F1 cells and 7 day old B16F1 melanomas (n=4 animals). *p<0.05, **p<0.01. **C,** Correlation between SDC4 expression and new blood vessels in the retinas of diabetic retinopathy patients. Multiple linear regression analysis of correlation between SDC4 and $CD31^{+}$ or $VEGFR2^{+}$ area (%) (Correlation R=0.751, p=0.036, coefficients CD31=0.963, VEGFR2=0.032). n=6 patients (2-3 sections per patient), individual ROIs (n=11) were used for the analysis.

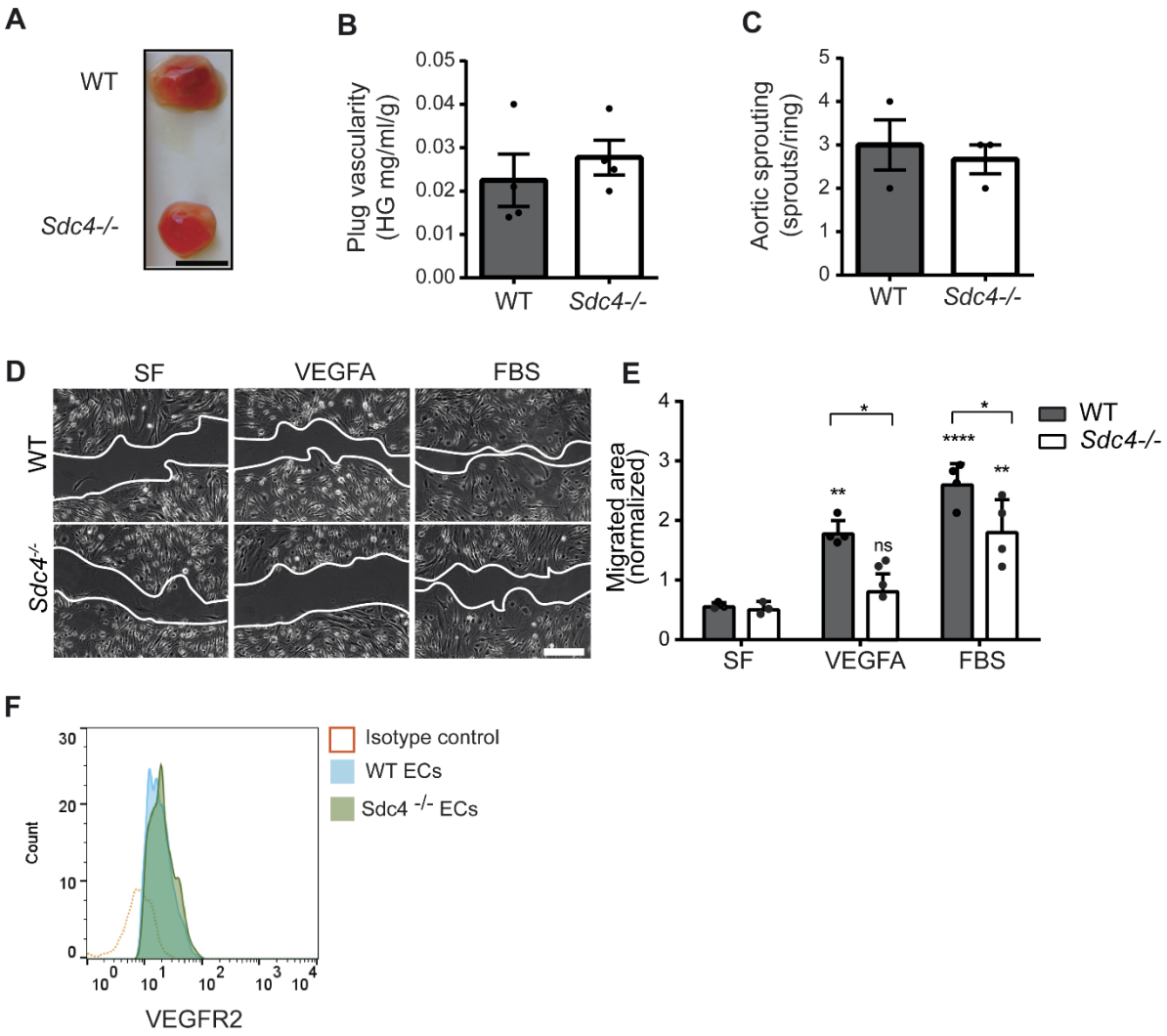

Figure V. FGF induced angiogenic responses are comparable between WT and *Sdc4-/-* animals. A, Matrigel supplemented with PBS or bFGF (50 ng) was injected subcutaneously in the flank of WT or *Sdc4-/-* mice. Images are representative of plugs extracted 7 days post-injection. Scale bar, 1 cm. **B,** Plug vascularity was expressed as the amount of haemoglobin released from the plugs per ml of Matrigel and normalized for the plug weight. n=5-6 animal for each group (2 plugs per animal). **C,** Aortic rings from WT and *Sdc4-/-* animals were treated with bFGF (50ng/ml). Data is mean of n=3 animals (10-18 rings/animal). **D,** Scratch wound migration assays comparing WT and *Sdc4-/-* MLECs either serum starved for 2 hours and stimulated with VEGFA or in complete media. **D,** Micrographs were obtained at 0 and 9 hours. **E,** Migrated area was calculated by subtracting the final scratch area from the initial scratch area using ImageJ. n=3-4, *p<0.05, **p<0.01, ****p<0.0001. **F,** Cell surface expression of VEGFR2 is the same on WT and *Sdc4-/-* MLECs as measured by flow cytometry. Primary ECs isolated from lungs of WT and *Sdc4-/-* were cultured for 2 weeks and analyzed by flow cytometry.

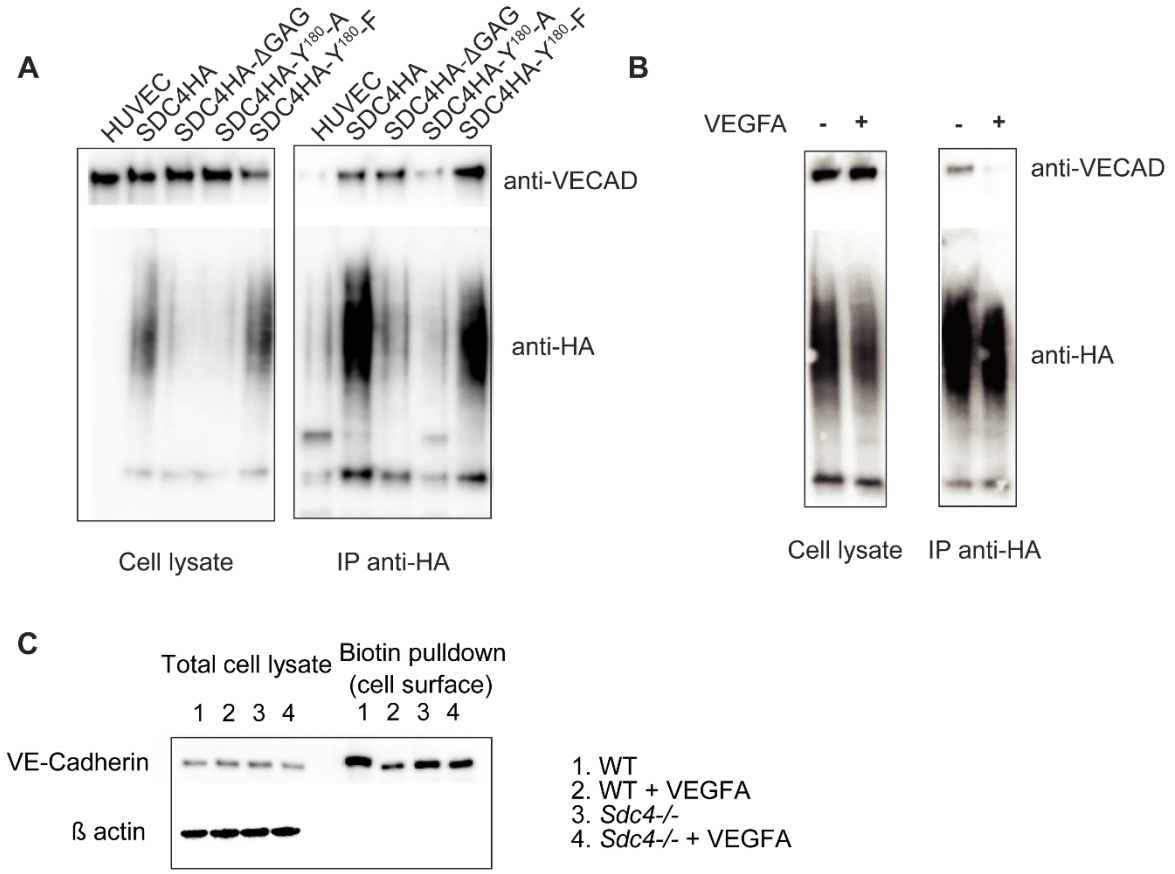

Figure VI. SDC4 interacts with VE-Cadherin under basal conditions, and this interaction is lost upon VEGFA stimulation. A, HUVECS were transduced with lentiviruses to express HA tagged versions of SDC4HA, SDC4HA-ΔGAG, SDC4HA-Y180-A and SDC4HA-Y180-F, and immuno-precipitation using anti-HA beads was performed on cell lysates. Western blot analysis was performed in immune-precipitates to look for the presence of VE-Cadherin. **B,** HUVECS transduced as described to express SDC4HA were serum starved for 2 hours prior to the addition of VEGFA (30 ng/ml, 20'). Immuno-precipitation was performed using anti-HA beads and analysed by western blot for the presence of VE-Cadherin. **C,** Serum starved (2hours) WT and *Sdc4-/-* MLECS were treated with and without VEGFA (10 ng/ml, 15'). Biotinylation of the cell surface proteins was performed and cells lysed and biotinylated proteins isolated using neutravidin beads. Lysates were analysed by western blot for the presence of VE-Cadherin. (Blots are representative of 3 independent experiments).

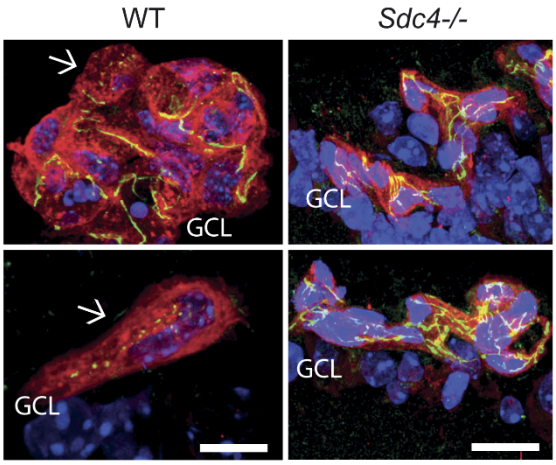

Figure VII. Reduced VE-Cadherin internalization in *Sdc4-/-* retinas after OIR. Two representative images of WT and *Sdc4-/-* OIR retinas paraffin-embedded, sectioned and stained with isolectin GS-IB4 (red), VE-Cadherin (green) and DAPI (blue). Arrows indicate VE-Cadherin+ vesicles. GCL: ganglion cell layer. Isolectin+ blood vessels are pre-retinal tufts. Scale bar, 20 μm.

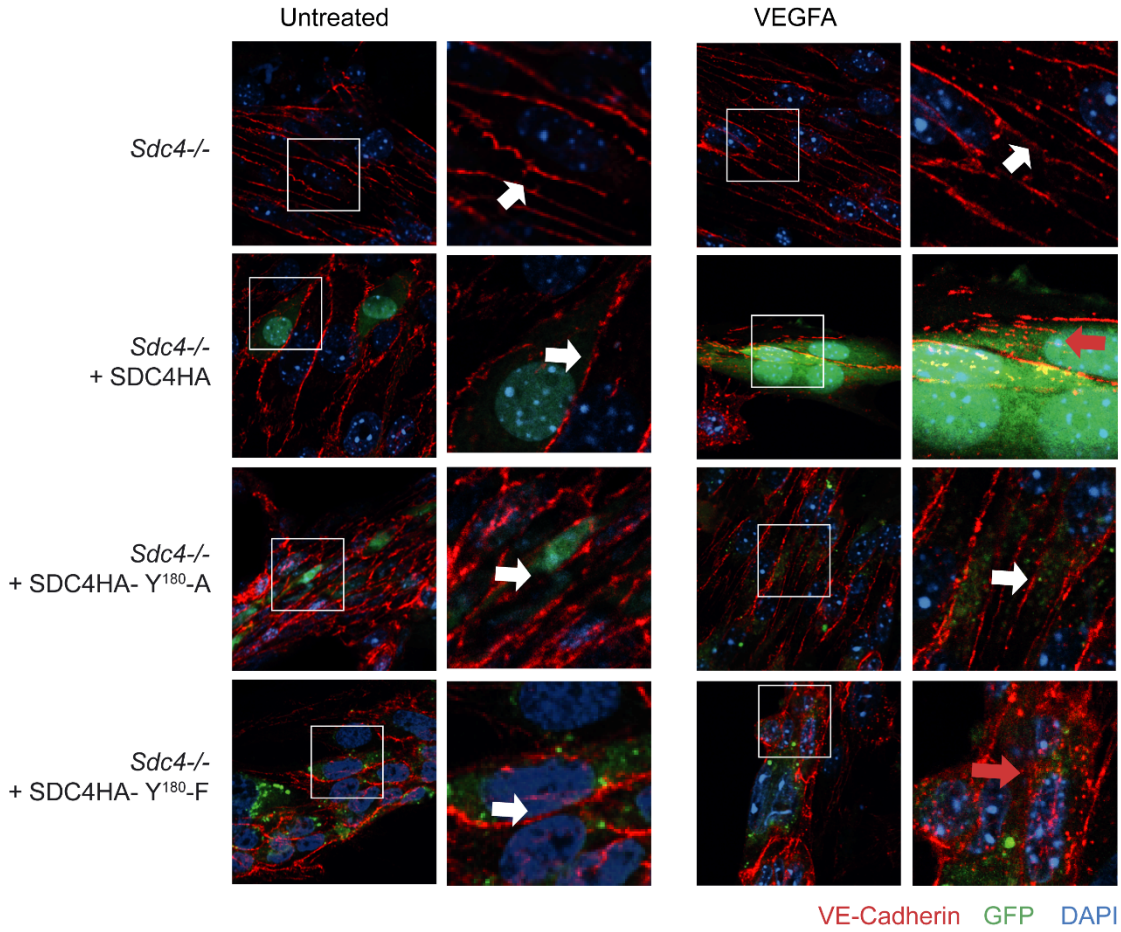

Figure VIII. Efficient VEGFA induced VE-Cadherin trafficking is restored in *Sdc4-/-* MLECs upon re-expression of SDC4. *Sdc4-/-* MLECs were lentivirally transduced to express either WT or mutant forms of SDC4 using a vector system containing an IRES element and eGFP downstream of the SDC4 cDNAs. Stably transfected cells were washed with PBS and incubated with anti-VE-Cadherin antibody at 4°C for 1 hour. Unbound antibody was removed prior to the stimulation of cells with VEGFA (30 ng/ml) for 10 mins at 37°C to promote VE-Cadherin internalization. Internalized VE-Cadherin positive vesicles are highlighted by red arrows, and junctional VE-Cadherin is indicated by white arrows.

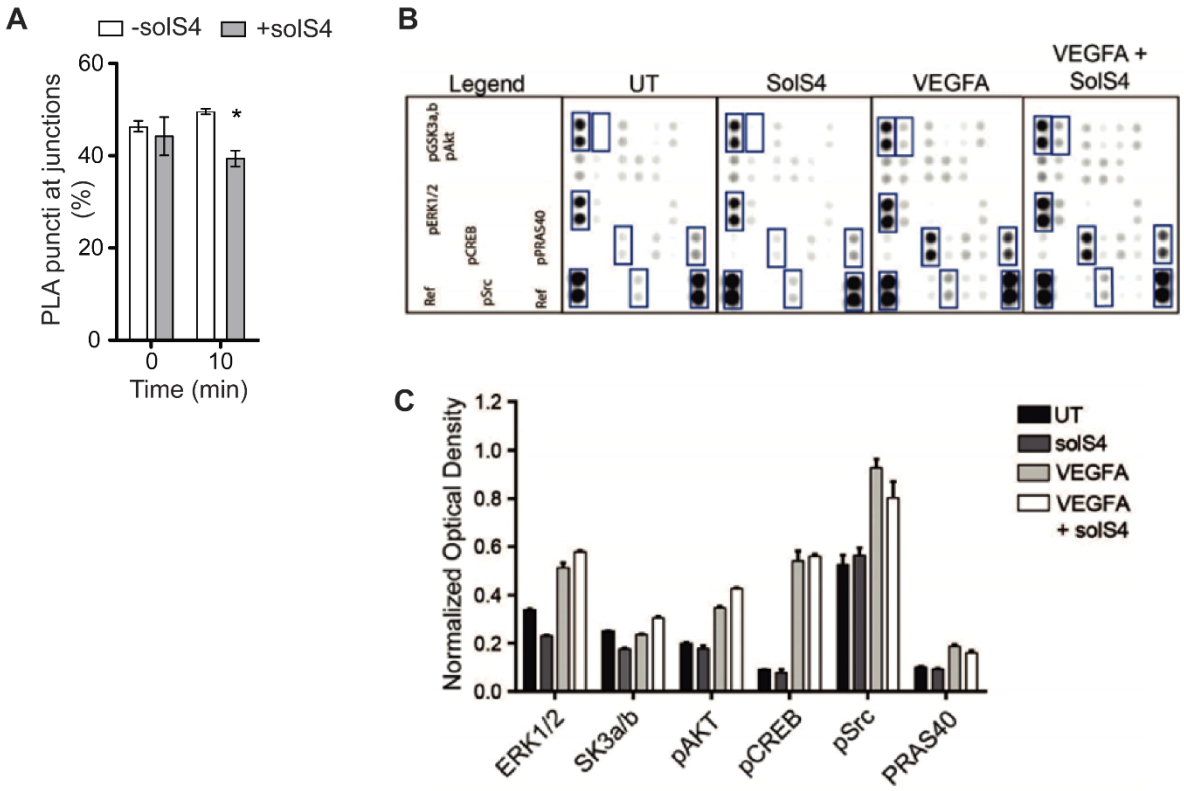

Figure IX. SolS4 disrupts PLA puncti between SDC4 and VE-Cadherin and has no impact on VEGFA signaling. A, SolS4 disrupts PLA puncti between SDC4 and VE-Cadherin at EC junctions. HUVECs were incubated with VEGFA (10 ng/ml) in the presence of SolS4 (3.5nM) for the time indicated prior to fixation and PLA analysis. 12-15 cells were analysed per condition. **B,** Confluent HUVECs were serum-starved for 2 hours and treated with soluble SDC4 (solS4, 3.5 nM), VEGFA (20 ng/ml) or both for 10 min. Lysates were then analyzed using a human phospho-kinase membrane-based sandwich immunoassay. **C,** Phosphorylated kinases were quantified using ImageJ, signals normalized using the reference spots. Phosphorylation sites were as follows, pERK1/2 (T202/Y204, $T^{185/Y187}$), pGSK-3a,b ($S^{21/S9}$), pAkt1/2/3 (S^{473}), pCREB (S^{133}), pSrc (Y^{419}), pPRAS40 (T^{246}).

SUPPLEMENTAL MATERIAL AND METHODS

Study design: The objective of animal studies described here was to evaluate the role of SDC4 in developmental angiogenesis, pathological neovascularization in the eye and in tumor models. Sample size was based on power calculations. In the laser induced CNV study, 7 represented the optimum number of animals needed to attain statistical significance of $p<0.05$ with a 90% probability given our pilot study values of 7 ±2 for group 1 and 4 ±1.5 for group 2. N was increased to 9 per group given the incidence of post-laser hemorrhage. The end-point of the experiment was day 7. Lesions that showed hemorrhage or two lesions fused together were excluded from analysis. For OIR experiments, 17 represented the minimum number of animals needed to attain statistical significance of $p<0.05$ with an 80% probability given our pilot study values of 4 ± 2 for group 1 and 2.5 ± 1 for group 2. N was increased to 21 per group. Three separate OIR experiments were performed and the end-point of the experiment was day 17. In developmental retinal angiogenesis study, 8 represented the optimum number of animals needed to attain statistical significance of $p<0.05$ with a 90% probability given our pilot study values of 30±4 for group 1 and 25±2 for group 2. N was increased to 9 per group. End-point of the experiment was day 6. Investigators were blinded during all phases of the experiments and genotypes or treatments groups only revealed after analysis.

List of reagents: The following dyes and reagents were used in this work; lectin GS-II Alexa594 (Thermo Fisher Cat#L21416), DAPI (Sigma-Aldrich, Cat#D9542), Draq5 (Biostatus limited Cat#DR05500), recombinant mouse VEGFA 164 (R&D Systems Cat#493-MV-025m), Bradykinin (Sigma Cat#B3259), recombinant syndecan-4 (R&D Systems Cat# 6267-SD-050) and recombinant syndecan-2 (R&D Systems Cat#6585-SD-050), proteome profiler human phospho-kinase array kit (R&D Systems Cat#ARY003B), Halt™ Protease and Phosphatase Inhibitor Single-Use Cocktail (100X) (Thermofisher Cat#78440), EZ-Link™ Sulfo-NHS-Biotin, No-Weigh™ Format (Thermofisher Cat#A39256), Pierce™ NeutrAvidin™ Agarose (Thermofisher Cat#29200).

Immunohistochemical (IHC) staining of papillomas: Samples of back skin from sacrificed, shaved control mice or mice at 43 hours or week 17 of the tumor induction experiment were collected and fixed with 4% paraformaldehyde and embedded in paraffin according to standard protocols. Hematoxylin/eosin staining and DAB immune-histochemical staining (IHC) was performed on 6 µm thick paraffin sections as previously described in[33]. Rat anti-CD31 (BD Pharmingen, Oxford, UK) primary antibody was used for IHC. The blocking reagents used for IHC were S2O23 REAL and S0809 Antibody Diluent (Dako). The horseradish peroxidase (HRP) conjugated secondary antibody used was 414311F anti-rat Histofine (Nichirei Bio, Tokyo, Japan) and peroxidase reactive chromogens used was K3465 DAB (DAKO).

Quantitative analysis of immunostaining and histochemical staining: All slides were scanned using the Aperio ScanScope® CS and XT systems (Aperio Technologies Inc., California, USA) as previously described[33]. Slides were viewed and analyzed remotely using desktop personal computers employing the web-based ImageScope™ viewer. The Spectrum digital pathology system analysis algorithm package and Image Scope analysis software (version 9; Aperio Technologies Inc.) were applied to quantify immune-histochemical signal. These algorithms calculate the area of positive staining, the average positive intensity (optical density), as well

as the percentage of weak (1+), medium (2+), and strong (3+) positive staining. The quantified CD31 expression was performed according to the protocols used to establish these algorithms for each respective staining[33]. Blood vessel diameter was determined from CD31-stained tissue sections by drawing a straight line from the outer edges of CD31-staining on all blood vessels with distinguishable lumen.

qPCR: RNA was purified using the Qiagen RNeasy Microkit as described by the manufacturers, cDNA was synthesized from 10 ng total RNA using the iScript cDNA synthesis kit (Biorad), quantitative real time PCR was performed on an ABI7900HT (Applied Biosystems) real time PCR machine using the iQ Sybr green supermix (Biorad). Sequences of primers used in this are as follows: Mouse syndecan-1 forward 5'-GGT GGA CGA AGG AGC CAC A-3', mouse syndecan-1 reverse 5'-CTC CGG CAA TGA CAC CTC C-3', mouse syndecan-2 forward 5'-GAG GCA GAA GAG ATG CTG G-3', mouse syndecan-2 reverse 5'-CAT CAA TGA CGG CTG CTA G-3', mouse syndecan-3 forward 5'-GCC CTG GCC TCC ACG AC-3', mouse syndecan-3 reverse 5'-CAC GAT CAC GGC TAC GAG C-3', mouse syndecan-4 forward 5'-CAC GAT CAG AGC TGC CAA G-3', mouse syndecan-4 reverse 5'GGA TGA CAT GTC CAA CAA AGT-3', mouse GAPDH forward 5'-TCG TGG ATC TGA CGT GCC GCC TG-3', mouse GAPDH reverse 5'-CAC CAC CCT GTT GCT GTA GCC GTA T-3'.

Human samples: Pre-retinal neovascular membranes were obtained from type I diabetic patients who were undergoing pars plana vitrectomy for the treatment of proliferative diabetic retinopathy. These patients had already developed tractional retinal detachment due to fibrosis of neovascular membranes. Thus, the samples represent the end stage disease, where substantial amount of fibrosis was associated with neovessels, but still contained regions with active pathologic angiogenesis. All patients were Caucasians, males and females, aged between 27–56 years, and mean duration of diabetes was 24 years (range, 21–28 years). The protocol for collecting human tissue samples was approved by the Institutional Review Boards of the Pirkanmaa Hospital District. The study was conducted in accordance with the Declaration of Helsinki. All patients gave written informed consent. During vitrectomy, the fibrovascular membranes were isolated, grasped with vitreous forceps, and pulled out through a sclerotomy. The sample was immediately fixed with 4 % formaldehyde for 3 h, transferred to 70 % ethanol, embedded in paraffin, and processed for immunohistochemistry. Adjacent 5 µm sections were stained for anti-CD31, anti-VEGFR2 and anti-SDC4 KY/8.2 followed by horseradish peroxidase (HRP) conjugated secondary antibodies. The slides were imaged via Olympus light microscope and Cell Sens Dimensions software. Quantification was done using IHC Profiler plugin in ImageJ 1.44p software (National Institutes of Health, Bethesda, MD). The same region of interest was selected from all stained sections (2-3 sections per sample) and the area (%) of total positive staining was quantified. To analyze the correlation between SDC4, VEGFR2 and CD31 positive area in each ROI, a multiple linear regression analysis was done in IBM SPSS Statistics.

Immunohistochemistry (IHC) and Isolectin GS-IB$_4$ Staining of mouse retinas: For the analysis of murine retinal vasculature, eyes were enucleated, fixed with 4% paraformaldehyde (PFA), and retinas dissected. Flat-mount retinas were blocked in 20% normal goat and 20% fetal bovine serums for 2 hours, incubated overnight Isolectin (Isolectin GS-IB$_4$, 1:200; Invitrogen, Carlsbad, CA, USA) and with anti-VE-

cadherin antibody, followed by Alexa Fluor-conjugated secondary antibody. The samples were mounted with Vectashield mounting medium with DAPI **(**Vector Laboratories, Burlingame, CA) and images were captred by confocal microscopy. (Carl Zeiss LSM 700).

Matrigel plug assay: Matrigel (400 µl, BD Biosciences) was thawed on ice and mixed with 100 µl PBS containing growth factors 100 ng/ml VEGFA and 20 U/ml of Heparin (Sigma) and injected subcutaneously into the flank of male anesthetized 6 week old mice roughly between the rib cage and the posterior leg. After 5 days, mice were sacrificed by cervical dislocation and plugs recovered after dissection. Plugs were imaged using a conventional digital camera, weighed on a precision balance and incubated overnight at 4 °C with 500 µl of dH_2O. The amount of hemoglobin released from the plugs was measured using the Drabkin reagent kit (Sigma) as described by the manufacturer. Absorbance at 540 nm was read using a spectrophotometer and results quantified using a standard curve of known concentrations of hemoglobin and data was expressed as the concentration of hemoglobin per gram of plug (HG mg/ml/g).

Choroid and aortic sprouting assay: Aortic rings were prepared from 6-8 week old male mice. Briefly, aortas were dissected, washed in PBS and fat and side branches were removed prior to slicing into rings (~1mm diameter) and these were incubated o/n in serum-free OptiMEM (containing Penicillin-Streptomycin) at 37 °C. Choroid explants were prepared from eyes, as follows; eyes were punctured with scissors, an incision was made 1 mm below the iris and the iris/cornea/lens/retina were removed. The choroid was cut into approximately 1 mm^2 pieces (~ 4 from central, 6 from periphery) and incubated o/n in OptiMEM, as above. Explants were embedded in 150 µl/well of a type I collagen matrix (1 mg/ml) in E4 media (Invitrogen) in a 48-well plate (Corning). Plates were incubated at 37 °C for 30 min to allow the collagen to solidify, after which time wells were supplemented with 200 µl OptiMEM with 1 % FBS and VEGFA (30 ng/ml) and incubated at 37 °C, 10 % CO2. Media was replenished every third day and angiogenic sprouts from aortic rings or choroid explants were counted after 1 week and results were expressed as the number of sprouts per ring or explant.

Primary mouse lung endothelial cell (MLEC) isolation and HUVEC culture: Cells were isolated and cultured from male WT and *Sdc4-/-* animals as described [29]. HUVECs were obtained from Promocell and were grown and maintained according to supplier's instructions in ECGM2 medium C-22111. RAW 246.7 macrophages were obtained from HPA culture laboratories (Public Health Laboratories, UK) and grown in DMEM supplemented with 10% FCS.

Migration assay: Cells were cultured in 6- or 12-well plates until confluent and serum starved for 3 hours. One longitudinal scratch was introduced to the monolayer with a sterile pipette tip, cells were then washed to remove debris and incubated in fresh medium. Regions of interests in the scratch area were recorded using Cell^M software (Olympus) and micrographs of ROIs taken every 30 min for 16 hours with an Olympus IX81 inverted microscope. The initial and final gap was measured using ImageJ software (NIH).

Lentiviral constructs: cDNA encoding the full-length sequence of murine SDC4 (Sdc4-eGFP) was synthesized to include either the complete coding sequence of eGFP or the HA epitope inserted between I^{32} and D^{33} of the extracellular domain. These provided the template to perform site directed mutagenesis to generate the various mutant forms of SDC4 used in this study. The cDNAs were ligated into the BamHI and XhoI sites of the lentiviral vector plentiSFFV-MCS using conventional procedures. Lentiviruses were packaged in HEK 293T cells under the control of the GagPol promoter using the VSVG envelope protein. HUVECs and MLECS were transfected by overnight incubation with viral preparations.

Immunoprecipitation and western blot. Confluent EC monolayers were lysed in TBS containing 1% v/v triton x100 and HALT phosphatase inhibitors (Thermo Fisher). Immuno-precipitation of HA tagged SD4 proteins was performed using anti-HA Agarose beads (Pierce). Beads and lysates were incubated o/n at 4°C and beads harvested by centrifugation. Beads were washed 3x with TBS prior to incubation in Laemmli buffer and analysis by western blot. Chemiluminescent detection of proteins was performed using an Azure c600 imaging system using the manufacturer's reagents.

Biotinylation: Primary MLECs (WT and *Sdc4-/-*) were starved for 1 hour in ECGM2 (without supplement or FBS and VEGFA was added (50 ng/ml for 15'). Cells were washed on ice twice with PBS (with Calcium and Magnesium), sulfo-NHS-biotin was dissolved in PBS at a concentration of 0.5 mg/ml and incubated with the cells for 20' on a shaker on ice. Cell were washed twice in PBS and blocked with complete ECGM2 for 20' on ice, after which lysates were made (lysis buffer composed of TBS, EDTA 10 mM, 1% tryton X100, phosphatase/protease inhibitor cocktail). A small volume was kept to represent whole lysates, while remaining sample was incubated with neutravidin-agarose for 2 hours at 4°C, centrifuged, washed 3 times with lysis buffer and resuspended in Laemmli buffer for western-blotting analysis.

Major Resources Table

In order to allow validation and replication of experiments, all essential research materials listed in the Methods should be included in the Major Resources Table below. Authors are encouraged to use public repositories for protocols, data, code, and other materials and provide persistent identifiers and/or links to repositories when available. Authors may add or delete rows as needed.

Animals (in vivo studies)

Species	Vendor or Source	Background Strain	Sex	Persistent ID / URL
Mouse	Charles River	C57BL/6J	m/f	
Mouse	CARD, Kunamoto university, Japan	C57BL/6J *Sdc4-/-*	m/f	

Antibodies

Target antigen	Vendor or Source	Catalog #	Working concentration	Lot # (preferred but not required)	Persistent ID / URL
VEGFR2	Santa cruz	6251	1 μg/ml		
VEGFR2	Cell signaling	2479	1:1000		
Syndecan-4	Abcam	24511	5 μg/ml		
Syndecan-4	eBiovision	3644	5 μg/ml	4AIIL36440	
CD31	BD Pharmingen	550274	1.5 μg/ml		
VE-Cadherin	Abcam	33168	1 μg/ml		
VE-Cadherin	eBioscience	14-1441-82	5 μg/ml		
VE-Cadherin	Santa cruz	9989	0.8 μg/ml	E1018	
Alpha-SMA	Sigma	A2547	1 μg/ml		
VEGFR2pY1175	Cell signaling	9698	1:1000		
Beta-tubulin	Sigma	T4026	0.1 μg/ml	043M4785	
VEGFR2-FITC	BD Pharmingen	560680	2.5 μg/ml	01750	
IgG2a,k-FITC	BD Pharmingen	553929	2.5 μg/ml		
Syndecan-4-PE	BD Pharmingen	550352	2.5 μg/ml	6204630	
IgG2a,k-PE	BD Pharmingen	553930	2.5 μg/ml		
Podocalyxin	R&D systems	AF1556	10 μg/ml		

Clone Name	Sequence	Source / Repository	Persistent ID / URL
pLNT-SFFV-SDC4HA	Murine SDC4 sequence with coding sequence for HA tag inserted between I^{31} and D^{32}	Made as part of this study contact Corresponding author	

pLNT-SFFV-SDC4ΔGAG	SDC4HA sequence mutated such that $S^{44,62,64}$ is mutated to Alanine.	Made as part of this study contact Corresponding author	
pLNT-SFFV-SDC4HA Y180-A	SDC4HA sequence mutated such that Y^{180}-A.	Made as part of this study contact Corresponding author	
pLNT-SFFV-SDC4HA Y180-F	SDC4HA sequence mutated such that Y^{180}-F.	Made as part of this study contact Corresponding author	
pLNT-SFFV-Sdc4eGFP	Murine SDC4 sequence with the complete cDNA for eGFP inserted between I^{31} and D^{32}.	Made as part of this study contact Corresponding author	
pLNT-SFFV-Sdc4eGFP Y-A	Sdc4eGFP mutated at Y^{180} to A.	Made as part of this study contact Corresponding author	
pLNT-SFFV-Sdc4eGFP Y-F	Sdc4eGFP mutated at Y^{180} to F.	Made as part of this study contact Corresponding author	

Cultured Cells

Name	Vendor or Source	Sex (F, M, or unknown)	Persistent ID / URL
Human umbilical vein endothelial cells (HUVECs)	Promocell	Mix donors pooled	
RAW 246.7 macrophages	HPA	male	